

See discussions, stats, and author profiles for this publication at: <https://www.researchgate.net/publication/51734255>

# Physiologically Relevant Concentrations of NaCl and KCl Increase DNA Photocleavage by an N-Substituted 9-Aminomethylanthracene Dye

ARTICLE in BIOCHEMISTRY · NOVEMBER 2011

Impact Factor: 3.02 · DOI: 10.1021/bi200972c · Source: PubMed

---

CITATIONS

5

---

READS

84

## 5 AUTHORS, INCLUDING:



María-José Fernández

University of Alcalá

22 PUBLICATIONS 158 CITATIONS

SEE PROFILE

# Physiologically Relevant Concentrations of NaCl and KCl Increase DNA Photocleavage by an N-Substituted 9-Aminomethylanthracene Dye

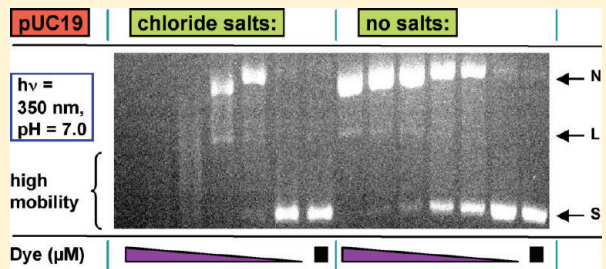
Carla A. Terry,<sup>†</sup> María-José Fernández,<sup>‡</sup> Lourdes Gude,<sup>‡</sup> Antonio Lorente,<sup>\*,‡</sup> and Kathryn B. Grant<sup>\*,†</sup>

<sup>†</sup>Department of Chemistry, Georgia State University, P.O. Box 4098, Atlanta, Georgia 30302-4098, United States

<sup>‡</sup>Departamento de Química Orgánica, Universidad de Alcalá, 28871-Alcalá de Henares, Madrid, Spain

Supporting Information

**ABSTRACT:** This paper describes the synthesis of a new 9-aminomethylanthracene dye N-substituted with a pyridinylpolyamine side chain (**4**). The effects of NaCl and KCl on anthracene/DNA interactions were then studied, with the goal of simulating the conditions of high ionic strength that a DNA photosensitizer might encounter in the cell nucleus (~150 mM of NaCl and 260 mM of KCl). As exemplified by methylene blue (**5**), the expected effect of increasing ionic strength is to decrease DNA binding and photocleavage yields. In contrast, the addition of 150 mM of NaCl in combination with 260 mM of KCl to photocleavage reactions containing micromolar concentrations of **4** triggers the conversion of supercoiled, nicked, and linear forms of pUC19 plasmid into a highly degraded band of DNA fragments (350 nm  $\text{h}\nu$ , pH 7.0). Circular dichroism spectra point to a correlation between salt-induced unwinding of the DNA helix and the increase in DNA photocleavage yields. The results of circular dichroism, UV-vis absorption, fluorescence emission, thermal denaturation, and photocleavage inhibition experiments suggest that the combination of salts causes a change in the DNA binding mode of **4** from intercalation to an external interaction. This in turn leads to an increase in the anthracene-sensitized production of DNA-damaging reactive oxygen species.



Anthracene dyes are aromatic hydrocarbons consisting of three fused six-membered rings. These versatile chromophores have been used as semiconducting materials,<sup>1</sup> in light-emitting diodes,<sup>2</sup> and as fluorescent sensors for analyte detection.<sup>3,4</sup> In biological systems, anthracenes bind avidly to DNA,<sup>5,6</sup> where they interact by intercalative and by groove-binding modes.<sup>7–9</sup> This has constituted the basis for their use as chemotherapeutic agents.<sup>5,6</sup> Thus, the anthracene derivatives mitoxantrone and/or bisantrene have been utilized in the treatment of metastatic breast cancer,<sup>10</sup> non-Hodgkin lymphoma,<sup>11</sup> acute lymphoblastic leukemia,<sup>12</sup> and metastatic prostate cancer.<sup>13</sup>

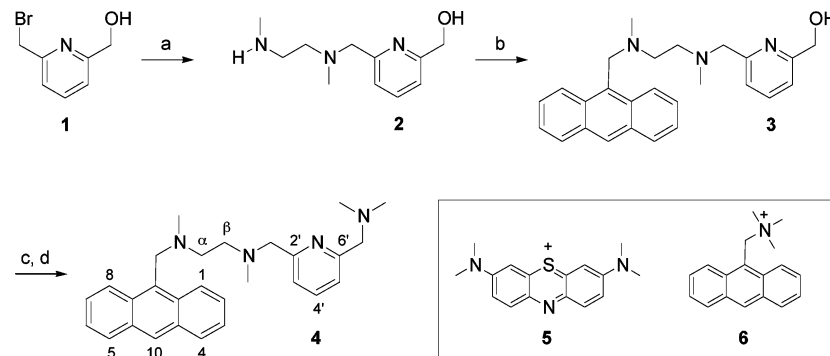
Upon the absorption of long wave ultraviolet light (UVA; 320–400 nm), anthracene dyes produce singlet oxygen ( ${}^1\text{O}_2$ ) and hydroxyl radicals ( ${}^\bullet\text{OH}$ ),<sup>14,15</sup> reactive oxygen species (ROS) that cause extensive photo-oxidative damage to DNA and to other macromolecules in living systems.<sup>16</sup> As a result, anthracene-based intercalators are among the different DNA photosensitizers that have displayed activity in phototherapeutic applications.<sup>14,17</sup> In the laboratory, anthracenes produce efficient degradation of DNA under the standard, low salt conditions routinely used in *in vitro* photocleavage reactions (0 mM NaCl to 50 mM NaCl<sup>8,15,18–21</sup>). Results were very favorable, and in several cases, near complete photoconversion of supercoiled plasmid DNA (S) to its nicked (N) and linear (L) forms was observed.<sup>8,15,20,21</sup>

Within the cell nucleus where genomic DNA is contained, the average concentrations of NaCl and KCl are considerably higher (approximately 150 and 260 mM, respectively)<sup>22–25</sup> compared to the standard *in vitro* concentrations (0 mM NaCl to 50 mM NaCl).<sup>8,15,18–21</sup> Thus, in phototherapeutic applications, an ideal DNA photosensitizer should continue to function optimally under the conditions of ionic strength that exist in the cell nucleus. This goal is formidable, however. Ligands that bind to double-helical DNA, through intercalation and/or association with the DNA grooves, typically lose their binding affinity as ionic strength is increased.<sup>8,26–28</sup> According to Manning's polyelectrolyte theory, monovalent cations such as  $\text{Na}^+$  and  $\text{K}^+$  interact with DNA through condensation and screening effects that stabilize the polyanionic duplex.<sup>29</sup> Although positively charged DNA ligands contribute to charge neutralization, they can be displaced by a competitive salt effect in which high concentrations of  $\text{Na}^+$  and  $\text{K}^+$  cations effectively compete for negatively charged binding sites.<sup>26</sup> It has also been proposed that the decrease in phosphate–phosphate repulsion that occurs under conditions of high ionic strength can promote ligand dissociation from DNA<sup>8</sup> by triggering structural changes<sup>30–33</sup> that include alterations in helical diameter<sup>32</sup> and

Received: June 24, 2011

Revised: October 17, 2011

Published: October 20, 2011

**Scheme 1. Synthesis of N-Substituted 9-Aminomethylanthracene 4<sup>a</sup>**

<sup>a</sup>Reagents and conditions: (a) to 2: *N,N'*-dimethylethylenediamine in CH<sub>3</sub>CN, add 1 in CH<sub>3</sub>CN dropwise over 3 h, then react 90 min, rt; (b) to 3: 9-chloromethylanthracene in CH<sub>3</sub>CN dropwise, then react 48 h, rt; (c) to 4: 3 in thionyl chloride, 12 h, rt, then (d) dry *in vacuo* and react with dimethylamine in MeOH, overnight, rt. Inset: structures of methylene blue (5) and (9-anthracenylmethyl)trimethylammonium chloride (6).

minor groove width.<sup>33</sup> In the case of DNA photosensitizing agents, the reduction in binding that occurs under conditions of high ionic strength has been shown to decrease DNA photocleavage yields.<sup>8,34–37</sup>

In this report, we describe the synthesis of a 9-amino-methylanthracene dye N-substituted with a pyridinylpolyamine side chain (4 in Scheme 1). The effects of high ionic strength on anthracene/DNA interactions are then studied. We have found that 4 is a very good DNA photocleaver but that cleavage efficiency is markedly enhanced upon the addition of 150 mM of NaCl and 260 mM of KCl to the DNA reactions. In the presence of the combination of chloride salts, near-complete photodegradation of pUC19 plasmid is observed at concentrations of 4 as low as 2.5 μM (350 nm, pH 7.0, 22 °C). We present evidence that the increase in DNA photocleavage is accompanied by a salt-induced change in anthracene interaction from intercalation to nonintercalative binding. This triggers an increase in the anthracene-sensitized production of DNA-damaging reactive oxygen species.

## EXPERIMENTAL PROCEDURES

**Materials and Methods.** Deionized, distilled water was utilized in the preparation of all buffers and aqueous solutions. Reagents were of the highest available purity and were used without further purification unless otherwise noted. Methylene blue chloride (99.99%, 5) was purchased from Fluka, and (9-anthracenylmethyl)trimethylammonium chloride (6) was from Aldrich. Sodium phosphate dibasic and sodium phosphate monobasic came from J.T. Baker and Fisher Scientific, respectively. Calf thymus DNA (CT DNA) was obtained from Invitrogen (Lot No. 15633-019, 10 mg/mL, average size ≤2000 bp). The DNA oligonucleotide 5'-CACTGGTCTCTAC-CAGTG-3' was purchased from Integrated DNA Technologies and then desalted using an Illustra NAP-25 column packed with Sephadex G-25 DNA grade resin (GE Healthcare). All other chemicals including copper<sup>2+</sup> chloride dihydrate, iron<sup>3+</sup> chloride hexahydrate, sodium chloride (99.999%), potassium chloride (99.999%), ethidium bromide, dimethyl sulfoxide (DMSO; >99.9%), sodium azide, sodium benzoate, D-mannitol, and deuterium oxide (99 atom % D) were from Sigma-Aldrich. The starting material 2-bromomethyl-6-hydroxypyridine (1) was prepared according to a reported procedure.<sup>38</sup>

Established literature protocols<sup>39</sup> were used to transform *E. coli* competent cells (Stratagene, XL-1 blue) with pUC19 plasmid DNA (Sigma-Aldrich) and to clone the plasmid in

bacterial cultures. Purification of the DNA was accomplished with a Quiagen Plasmid Mega Kit.

Thin-layer chromatography was performed on precoated aluminum silica gel plates (Machery-Nagel F<sub>254</sub> 0.2 mm). Merck silica gel 60 (70–230 ASTM mesh) was utilized for flash column chromatography. An FT-IR Perkin-Elmer 2000 spectrophotometer was used to plot infrared spectra. <sup>1</sup>H and <sup>13</sup>C NMR spectra were recorded at 300 MHz on Varian UNITY-300 and Varian Mercury-VX-300 instruments. The residual peaks of chloroform ( $\delta$  7.26 and 77.0 ppm) were employed as an internal NMR reference. An Automass Multi GC/API/MS Finnigan spectrometer was utilized to acquire ESI (electrospray ionization) mass spectra. UV-vis and fluorescence spectra were recorded with a UV-2401 PC spectrophotometer and an RF-1501 spectrofluorometer, respectively (Shimadzu Scientific Instruments). A Cary 300 Bio UV-vis spectrophotometer fitted with a Cary temperature controller was utilized to plot thermal melting curves. Circular dichroism (CD) and induced circular dichroism (ICD) spectra were acquired using a Jasco J-810 spectropolarimeter. Photocleavage reactions were run in an aerobically ventilated Rayonet photochemical reactor fitted with either ten RPR-3500 Å lamps or eight RPR-5750 Å lamps (The Southern New England Ultraviolet Co.). Elemental analyses (CHN) were done on a Perkin-Elmer 240-B analyzer.

**Synthesis of (6-((Methyl(2-(methylamino)ethyl)-amino)methyl)pyridin-2-yl)methanol (2).** *N,N'*-Dimethylethylenediamine (1.5 mL, 20 mmol) and anhydrous potassium carbonate (400 mg, 2.9 mmol) were transferred to dry acetonitrile (25 mL). To this suspension, a solution of 2-bromomethyl-6-hydroxypyridine<sup>38</sup> (1; 300 mg, 1.48 mmol) in dry acetonitrile (20 mL) was added dropwise for 3 h. The reaction mixture was stirred at rt for 90 min and then concentrated to dryness *in vacuo*. The white residue thus obtained was treated with distilled water (10 mL) and with an aqueous saturated sodium chloride solution (5 mL). The resulting suspension was extracted with dichloromethane (4 × 10 mL), and the combined organic extracts were dried with magnesium sulfate, filtered, and concentrated under reduced pressure to afford 340 mg (90%) of an oily product (2). <sup>1</sup>H NMR (CDCl<sub>3</sub>):  $\delta$  2.27 (s, 3H, NHCH<sub>3</sub>), 2.41 (s, 3H, NCH<sub>3</sub>), 2.57 (t,  $J$  = 5.9 Hz, 2H, CH<sub>2</sub> $\alpha$ ), 2.67 (t,  $J$  = 5.9 Hz, 2H, CH<sub>2</sub> $\beta$ ), 3.67 (s, 2H, PyCH<sub>2</sub>N), 4.71 (s, 2H, PyCH<sub>2</sub>OH), 7.10 (d,  $J$  = 7.7 Hz, 1H, H-3'), 7.25 (d,  $J$  = 7.7 Hz, 1H, H-5'), 7.63 (t,  $J$  = 7.7 Hz, 1H, H-4') ppm. <sup>13</sup>C NMR (CDCl<sub>3</sub>):  $\delta$  36.3, 42.6, 49.2, 56.6, 63.7,

64.0, 118.7, 121.4, 137.0, 158.3, 158.5 ppm. MS (ESI)  $m/z$  210 [ $M + H$ ]<sup>+</sup> (calcd for C<sub>11</sub>H<sub>20</sub>N<sub>3</sub>O 210.2). Anal. Calcd for C<sub>11</sub>H<sub>19</sub>N<sub>3</sub>O: C, 63.13; H, 7.64; N, 20.08. Found: C, 63.41; H, 7.56; N, 19.82.

**Synthesis of (6-((2-((Anthracen-9-ylmethyl)(methyl)amino)ethyl)(methyl)amino)methyl)pyridin-2-yl-methanol (3).** Compound 2 (104 mg, 0.5 mmol) and anhydrous potassium carbonate (100 mg, 0.72 mmol) were suspended in dry acetonitrile (10 mL). Then, a solution of 0.5 mmol (113 mg) of 9-chloromethylanthracene in dry acetonitrile (20 mL) was added dropwise. The reaction mixture was stirred at rt for 48 h and then concentrated *in vacuo* until dry. The resulting white residue was treated with distilled water (10 mL) and an aqueous saturated sodium chloride solution (5 mL). The suspension obtained was extracted with dichloromethane (4  $\times$  10 mL). The combined organic extracts were then dried with magnesium sulfate, filtered, and concentrated under reduced pressure to give a crude product. Purification was achieved by flash column chromatography in silica gel using ethyl acetate and then ethyl acetate-MeOH-triethylamine (10/2/1, v/v/v) as eluents. The combined fractions obtained with the last eluent were concentrated to dryness, affording the desired product 3 as an amber oil in 75% yield. IR (film):  $\nu$  2917, 2847, 2364, 1593, 1577, 1453, 1284, 1096 cm<sup>-1</sup>. <sup>1</sup>H NMR (CDCl<sub>3</sub>):  $\delta$  2.21 (s, 3H,  $\beta$ NCH<sub>3</sub>), 2.27 (s, 3H,  $\alpha$ NCH<sub>3</sub>), 2.70 ( $t$ ,  $J$  = 6.6 Hz, 2H, CH<sub>2</sub> $\beta$ ), 2.79 ( $t$ ,  $J$  = 6.6 Hz, 2H, CH<sub>2</sub> $\alpha$ ), 3.64 (s, 2H, NCH<sub>2</sub>Py), 4.46 (s, 2H, CH<sub>2</sub> Anthr), 4.70 (s, 2H, PyCH<sub>2</sub>OH), 7.04 (d,  $J$  = 7.6 Hz, 1H, H-3'), 7.14 (d,  $J$  = 7.6 Hz, 1H, H-5'), 7.45 (m, 4H, H-2, H-3, H-6, and H-7), 7.53 (t,  $J$  = 7.6 Hz, 1H, H-4'), 7.98 (dd,  $J$  = 7.6, 1.8 Hz, 2H, H-4, and H-5), 8.40 (s, 1H, H-10), 8.50 (d,  $J$  = 8.1 Hz, 2H, H-1 and H-8) ppm. <sup>13</sup>C NMR (CDCl<sub>3</sub>):  $\delta$  42.4, 42.8, 54.1, 55.5, 56.0, 63.5, 63.8, 118.4, 121.5, 124.7, 125.1, 125.5, 127.4, 128.9, 130.2, 131.3, 131.4, 136.9, 157.8, 158.4 ppm. MS (ESI)  $m/z$  400 [ $M + H$ ]<sup>+</sup> (calcd for C<sub>26</sub>H<sub>30</sub>N<sub>3</sub>O 400.2). Anal. Calcd for C<sub>26</sub>H<sub>29</sub>N<sub>3</sub>O: C, 78.16; H, 7.32; N, 10.52. Found: C, 77.8; H, 7.49; N, 10.73.

**Synthesis of N-(Anthracen-9-ylmethyl)-N'-(6-((dimethylamino)methyl)pyridin-2-yl)methyl)-N,N'-dimethylethane-1,2-diamine (4).** To a round-bottomed flask with a trap of potassium hydroxide, 150 mg (0.375 mmol) of 3 and thionyl chloride (3 mL) were added. The orange solution was stirred at rt for 12 h. The thionyl chloride was then removed *in vacuo*, affording an orange solid that was dissolved in methanol. A 2 M solution of dimethylamine in methanol (2 mL, 4 mmol) was then added in one portion, and the reaction was stirred at room temperature overnight. After the methanol was evaporated under reduced pressure, the oily residue thus obtained was purified by flash column chromatography in silica gel using ethyl acetate and then ethyl acetate-triethylamine (95/5, v/v) as eluents. The combined fractions from the last eluent were concentrated until dryness, affording the desired product 4 (83 mg) as an amber oil in 70% yield. IR (film):  $\nu$  2917, 2848, 2360, 2341, 1655, 1591, 1453 cm<sup>-1</sup>. <sup>1</sup>H NMR (CDCl<sub>3</sub>):  $\delta$  2.21 (s, 3H,  $\beta$ NCH<sub>3</sub>), 2.24 (s, 3H,  $\alpha$ NCH<sub>3</sub>), 2.28 (s, 6H, NMe<sub>2</sub>), 2.69 ( $t$ ,  $J$  = 6.6 Hz, 2H, CH<sub>2</sub> $\beta$ ), 2.80 ( $t$ ,  $J$  = 6.6 Hz, 2H, CH<sub>2</sub> $\alpha$ ), 3.56 (s, 2H, PyCH<sub>2</sub>NMe<sub>2</sub>), 3.67 (s, 2H, NCH<sub>2</sub>Py), 4.46 (s, 2H, CH<sub>2</sub> Anthr), 7.18 (d,  $J$  = 7.6 Hz, 1H, H-3'), 7.23 (d,  $J$  = 7.6 Hz, 1H, H-5'), 7.45 (m, 4H, H-2, H-3, H-6, and H-7), 7.54 ( $t$ ,  $J$  = 7.6 Hz, 1H, H-4'), 7.98 (dd,  $J$  = 7.6, 2.0 Hz, 2H, H-4 and H-5), 8.40 (s, 1H, H-10), 8.50 (d,  $J$  = 8.1 Hz, 2H, H-1 and H-8) ppm. <sup>13</sup>C NMR (CDCl<sub>3</sub>):  $\delta$  42.3, 42.8, 45.5, 54.1, 55.5, 56.0, 63.9, 65.7, 121.2, 121.3, 124.7, 125.0,

125.6, 127.3, 128.9, 130.2, 131.3, 131.4, 136.6, 158.3, 159.0 ppm. HRMS (ESI)  $m/z$  427.2852 [ $M + H$ ]<sup>+</sup> (calcd for C<sub>28</sub>H<sub>35</sub>N<sub>4</sub> 427.2862). Anal. Calcd for C<sub>28</sub>H<sub>34</sub>N<sub>4</sub>: C, 78.83; H, 8.03; N, 13.13. Found: C, 78.60; H, 8.21; N, 13.22.

**Photocleavage of Supercoiled Plasmid DNA.** In concentration titration experiments, 10, 5, 2.5, 1.0, 0.5, and 0  $\mu$ M amounts of a dye, either N-substituted 9-aminomethylanthracene 4, methylene blue (5), or (9-anthracyl methyl)-trimethylammonium chloride (6), were equilibrated with 38  $\mu$ M bp of pUC19 plasmid DNA and 10 mM sodium phosphate buffer pH 7.0, in the presence and absence of 150 mM of NaCl in combination with 260 mM KCl, 150 mM NaCl, 260 mM KCl, or 410 mM NaCl (40  $\mu$ L total volume). Additional concentration titrations were conducted in which 10 to 0  $\mu$ M amounts of 4 were equilibrated with 38  $\mu$ M bp of pUC19 plasmid DNA in 150 mM NaCl, 260 mM KCl, and 10 mM sodium phosphate buffer, pH 7.0, in the presence and absence of 10  $\mu$ M CuCl<sub>2</sub>·2H<sub>2</sub>O or 10  $\mu$ M FeCl<sub>3</sub>·6H<sub>2</sub>O. In the above experiments, samples were kept for 1 h in the dark at 22 °C and were then irradiated for 60 min in an aerobically ventilated Rayonet photochemical reactor fitted with either ten RPR-3500 Å lamps (compounds 4 and 6) or eight RPR-5750 Å lamps (compound 5). Parallel control reactions consisting of 10 mM sodium phosphate buffer, pH 7.0, 38  $\mu$ M bp of pUC19, and 10  $\mu$ M dye were prepared in the presence and absence of the appropriate amounts of the copper<sup>2+</sup>, iron<sup>3+</sup>, potassium<sup>+</sup>, and sodium<sup>+</sup> chloride salts. The control reactions were kept in the dark during the 60 min irradiation period (no  $h\nu$ ).

In time course experiments, 2.5  $\mu$ M N-substituted 9-aminomethylanthracene 4 was equilibrated with 38  $\mu$ M bp of pUC19 plasmid DNA and 10 mM sodium phosphate buffer, pH 7.0, in the presence and absence of 150 mM NaCl in combination with 260 mM KCl (40  $\mu$ L total volume). The individual 40  $\mu$ L reactions were irradiated in the Rayonet photochemical reactor for specific time intervals ranging from 5 to 60 min (350 nm, 22 °C).

After irradiation, a total of 3  $\mu$ L of electrophoresis loading buffer (15.0% (w/v) Ficoll, 0.025% (w/v) bromophenol blue) was transferred to each 40  $\mu$ L cleavage reaction. The samples were then loaded onto 1.5% nondenaturing agarose gels stained with ethidium bromide (0.5  $\mu$ g/mL, final concentration) and electrophoresed at 160 V using 1  $\times$  TAE running buffer in an OWL A1 large gel system (Thermo Scientific). Gels were visualized on a transilluminator set at 302 nm and photographed. For time course, scavenger, and D<sub>2</sub>O experiments, the gels were quantitated with ImageQuant v. 5.0 software. The data obtained for supercoiled DNA were multiplied by a correction factor of 1.22 in order to account for the decreased binding affinity of ethidium bromide to supercoiled vs nicked and linear plasmid forms. Photocleavage yields were then calculated according to formula 1.

percent photocleavage

$$= [( \text{linear} + \text{nicked DNA}) / (\text{linear} + \text{nicked} + \text{supercoiled DNA})] \times 100 \quad (1)$$

**Circular Dichroism Analysis.** Individual CD samples consisted of 10 mM sodium phosphate buffer, pH 7.0, in the presence and absence of one or more of the following reagents: 10  $\mu$ M 4, 30  $\mu$ M bp of calf thymus DNA, 150 mM NaCl, and 260 mM KCl (700  $\mu$ L total volume). For ICD spectra, samples contained 10 mM sodium phosphate buffer, pH 7.0, 50  $\mu$ M 4,

and/or 150  $\mu\text{M}$  bp of CT DNA in the presence and absence of 150 mM NaCl and 260 mM KCl (2000  $\mu\text{L}$  total volume). After equilibration in the dark for 1 h at 22 °C, CD and ICD spectra were collected using 1 mL (0.2 cm) and 3 mL (1.0 cm) quartz cuvettes (Starna), respectively. The following operating parameters were employed: scan rate, 100 nm/min; response time, 1 s; bandwidth, 1 nm; and sensitivity, 100 mdeg. The final spectra were averaged over four acquisitions.

**UV-vis Absorption Titrations.** In DNA titration experiments, small volumes of a 2000  $\mu\text{M}$  bp aqueous stock solution of CT DNA were sequentially added to anthracene samples containing 10 mM sodium phosphate buffer, pH 7.0, and 50  $\mu\text{M}$  compound 4 (500  $\mu\text{L}$  initial volume). Separate titrations were conducted in the absence and presence of 150 mM NaCl in combination with 260 mM KCl. Final concentrations of CT DNA ranged from 0  $\mu\text{M}$  bp up to 300  $\mu\text{M}$  or 400  $\mu\text{M}$  bp. In a third titration, small volumes of neat dimethyl sulfoxide were sequentially added to an anthracene sample containing 10 mM sodium phosphate buffer, pH 7.0, 50  $\mu\text{M}$  compound 4, 150 mM NaCl, and 260 mM KCl (500  $\mu\text{L}$  initial volume, no DNA used). The final concentrations of DMSO were from 0% (v/v) to 10% (v/v). After each sequential addition of titrant, the anthracene samples were equilibrated in the dark for 1 h at 22 °C, after which UV-vis absorption spectra were recorded from 800 to 200 nm at 22 °C. All absorption spectra were corrected for sample dilution.

**Fluorescence Measurements.** Samples consisted of 10 mM sodium phosphate buffer, pH 7.0, and 50  $\mu\text{M}$  4 in the presence and absence of one or more of the following reagents: 400  $\mu\text{M}$  bp of calf thymus DNA, 150 mM NaCl, and 260 mM KCl (2000  $\mu\text{L}$  total volume). After equilibration in the dark for 1 h at 22 °C, the anthracene solutions were excited at 393 nm in a 3 mL (1.0 cm) quartz cuvette (Starna). Fluorescence emission spectra were recorded from 250 to 700 nm at 22 °C.

**Thermal Denaturation Experiments.** DNA thermal melting curves were acquired as a function of increasing anthracene concentration. Solutions contained 0–54 or 72  $\mu\text{M}$  4, 30  $\mu\text{M}$  bp of the 18-mer DNA oligonucleotide 5'-CACTGGTCTCTACCAGTG-3', and 10 mM sodium phosphate buffer, pH 7.0, in either the absence or presence of 150 mM NaCl in combination with 260 mM KCl. Additional solutions consisting of 0–36  $\mu\text{M}$  concentrations of 4, 30  $\mu\text{M}$  bp of CT DNA, and 10 mM sodium phosphate buffer, pH 7.0, were prepared without the chloride salts. In a third experiment, thermal melting curves were recorded using 30  $\mu\text{M}$  bp of CT DNA and 10 mM sodium phosphate buffer, pH 7.0, with a fixed concentration of chromophore, either 0 or 10  $\mu\text{M}$  compound 4 or of methylene blue (5), in the presence and absence of individual salts, either 150 mM NaCl or 150 mM KCl. The solutions (1 mL total volume) were transferred to a 1.5 mL (1 cm) quartz cuvette (Starna) and were allowed to equilibrate for 1 h at 22 °C. Absorbance at 260 nm was then recorded as the temperature was increased from 25 to 95 °C at a heating rate of 0.5 °C/min. KaleidaGraph version 4.0 software was used to curve fit the first derivative of  $\delta A_{260}/\delta T$  vs temperature, where the melting temperature ( $T_m$ ) value was indicated by the maximum of each first-derivative plot.

**Chemically Induced Changes in DNA Photocleavage.** Individual reactions contained compound 4, 38  $\mu\text{M}$  bp of pUC19 plasmid DNA, 10 mM sodium phosphate buffer, pH 7.0, 100 mM singlet oxygen scavenger sodium azide, 100 mM hydroxyl radical scavenger sodium benzoate, 100 mM hydroxyl radical scavenger D-mannitol, or 81% (v/v) of D<sub>2</sub>O, in the

presence and absence of 150 mM NaCl in combination with 260 mM KCl. The final concentrations of compound 4 in the scavenger and D<sub>2</sub>O reactions were 2.5 and 0.2  $\mu\text{M}$ , respectively. In a set of parallel controls, sodium azide, sodium benzoate, D-mannitol, and D<sub>2</sub>O were replaced by equivalent volumes of ddH<sub>2</sub>O. All samples were pre-equilibrated in the dark for 1 h at 22 °C and then irradiated for 60 min at 22 °C in an aerobically ventilated Rayonet photochemical reactor fitted with ten RPR-3500 Å lamps. After irradiation, cleaved plasmid DNA was electrophoresed on a 1.5% nondenaturing agarose gel stained with ethidium bromide (0.5  $\mu\text{g}/\text{mL}$  final concentration). Gels were placed on a transilluminator set at 302 nm, photographed, and then quantitated using ImageQuant v. 5.0 software. The percent totals of supercoiled, nicked, and linear plasmid DNAs within each gel lane were determined. Photocleavage yields were calculated according to formula 1. In the case of the ROS scavengers, the percent inhibition of DNA photocleavage was calculated using formula 2.

percent photocleavage inhibition

$$\begin{aligned} &= [(\% \text{total of linear and nicked DNA}_{\text{without scavenger}} \\ &\quad - \% \text{total of linear and nicked DNA}_{\text{with scavenger}}) \\ &\quad / (\% \text{total of linear and nicked DNA}_{\text{without scavenger}})] \\ &\quad \times 100 \end{aligned} \quad (2)$$

## ■ RESULTS AND DISCUSSION

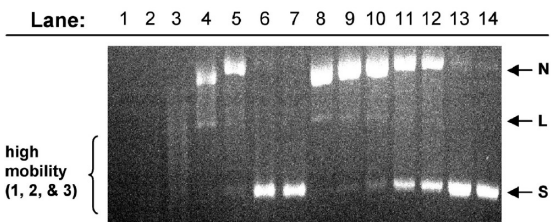
**Synthesis of N-Substituted 9-Aminomethylanthracene 4.** The design of 4 was based on placement of a positively charged pyridinylpolyamine side chain at the 9-position of an anthracene ring. Intercalative binding of anthracene with its long axis superimposed over the long axis of the DNA base pairs would place substituents at this position into one of the two DNA grooves.<sup>9</sup> In the case of 4, we envisaged that this might allow the positively charged ammonium groups in the side chain to participate in hydrogen bonding and electrostatic interactions with the DNA duplex.<sup>40</sup> Additionally, the incorporation of a potentially tridentate, metal-binding bis((dimethylamino)methyl)pyridine ring into the side chain of 4<sup>41</sup> might lead to metal complexation and/or to the formation of additional hydrogen bonds between the pyridine nitrogen atom and the 2-amino group of guanine.<sup>42</sup>

Synthesis of N-substituted 9-aminomethylanthracene 4 was carried out as shown in Scheme 1. Treatment of 2-bromomethyl-6-hydroxymethylpyridine (1)<sup>38</sup> with *N,N'*-dimethyl-ethylenediamine in dry acetonitrile afforded compound 2 in 90% yield. N-substituted 9-aminomethylanthracene 3 was then obtained by reacting 2 with 9-chloromethylanthracene in dry acetonitrile (75% yield). Treatment of 3 with neat thionyl chloride gave the corresponding alkyl chloride. Following the removal of the thionyl chloride *in vacuo*, reaction with dimethylamine in methanol afforded N-substituted 9-aminomethylanthracene 4 as the final product (70% yield). The structures of 2, 3, and 4 were confirmed from analyses of their <sup>1</sup>H and <sup>13</sup>C NMR, IR, ESI-MS spectral, and microanalytical data.

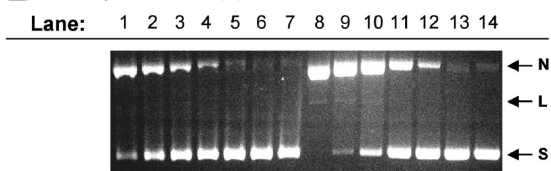
**Photocleavage of Plasmid DNA.** The effects of salt on DNA photocleavage were studied first. In these experiments, concentrations of NaCl and KCl were set at 150 and 260 mM, respectively, in order to simulate the conditions of high ionic strength that exist in the cell nucleus.<sup>22–25</sup> In a typical reaction, pUC19 plasmid DNA was equilibrated with either 10.0, 5.0, 2.5,

1.0, or 0.5  $\mu\text{M}$  concentrations of **4** in the presence and absence of 150 mM NaCl and 260 mM KCl (10 mM sodium phosphate buffer, pH 7.0). For comparison purposes, a parallel set of reactions was conducted using the intercalating dye methylene blue (**5** in Scheme 1). Uncleaved, supercoiled plasmid was changed to its nicked and linear forms by irradiation of the DNA samples (350 nm, 60 min). Reaction products were then resolved on 1.5% nondenaturing agarose gels (Figure 1).

**A) N-Substituted 9-(aminomethyl)anthracene **4****



**B) Methylene Blue (**5**)**



**C) 9-(Anthracenylmethyl)trimethylammonium Chloride (**6**)**

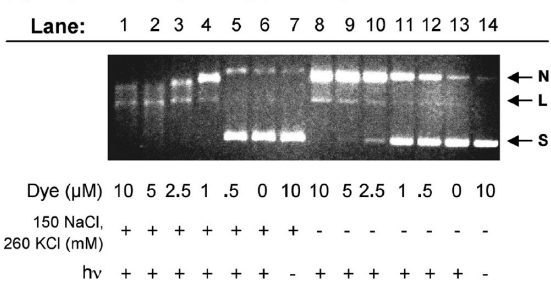


**Figure 1.** Photographs of 1.5% nondenaturing agarose gels showing photocleavage of 38  $\mu\text{M}$  bp of pUC19 plasmid by (A) N-substituted 9-(aminomethyl)anthracene **4**, (B) methylene blue (**5**), and (C) (9-anthracenylmethyl)trimethylammonium chloride (**6**). Samples contained 10 mM sodium phosphate buffer pH 7.0 and 38  $\mu\text{M}$  bp DNA. Lanes 1–6: 10 to 0  $\mu\text{M}$  of dye in the presence of 150 mM NaCl and 260 mM KCl. Lanes 8–13: 10 to 0  $\mu\text{M}$  of dye in the absence of 150 mM NaCl and 260 mM KCl. Lane 7: 10  $\mu\text{M}$  dye in the presence of 150 mM NaCl and 260 mM KCl (no  $\text{hv}$ ). Lane 14: 10  $\mu\text{M}$  dye in the absence of 150 mM NaCl and 260 mM KCl (no  $\text{hv}$ ). Prior to photocleavage, the reactions were pre-equilibrated for 1 h in the dark at 22 °C. The samples in Lanes 1–6 and 8–13 were irradiated at 350 nm (compounds **4** and **6**) or at 575 nm (compound **5**) for 60 min (22 °C). Abbreviations: L = linear; N = nicked; S = supercoiled.

As expected, the addition of the combination of salts inhibited DNA photocleavage by methylene blue at all dye concentrations (lanes 1 to 5 vs 8 to 12 in Figure 1B). In contrast, the combination of 150 mM NaCl and 260 mM KCl produced a dramatic enhancement in DNA photocleavage by N-substituted 9-aminomethylanthracene **4** (lanes 1 to 5 vs 8 to 12 in Figure 1A). The increase was evident even at the lowest concentration of **4** tested (0.5  $\mu\text{M}$ ), where the inclusion of the salts converted supercoiled and nicked forms of the plasmid to 100% nicked DNA (lanes 5 vs 12 in Figure 1A). In the presence

of 1.0  $\mu\text{M}$  **4**, supercoiled and nicked plasmid was changed to nicked and linear (lanes 4 vs 11 in Figure 1A). At higher concentrations of **4** (10.0, 5.0, and 2.5  $\mu\text{M}$ ), 150 mM NaCl and 260 mM KCl caused complete photodegradation of the plasmid into a diffuse band of high mobility DNA fragments (lanes 1 to 3 vs 8 to 10 in Figure 1A). No DNA photocleavage occurred when the plasmid was irradiated in the absence of dye (350 nm, 60 min; lanes 6 and 13 in Figure 1A,B) and when the highest concentration of **4** or **5** (10  $\mu\text{M}$ ) was reacted with the plasmid in the dark (no  $\text{hv}$ , 60 min; lanes 7 and 14 in Figure 1A,B).

The aim of our next experiment was to quantitate the amounts of DNA photocleavage produced by 9-aminomethylanthracene **4** as a function of time. Individual reactions contained 2.5  $\mu\text{M}$  **4**, the lowest concentration of dye to have produced near-complete photodegradation of the plasmid DNA (lane 3 in Figure 1A). After the samples were equilibrated in the presence and absence of 150 mM NaCl in combination with 260 mM KCl, they were irradiated at 350 nm for intervals of time up to 60 min (Figure S1 in the Supporting Information). DNA photocleavage yields were then determined by quantitating a photograph of the 1.5% agarose gel (Figure 2).

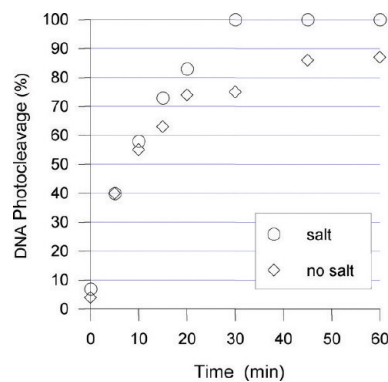


**Figure 2.** Time course plots for DNA photocleavage by N-substituted 9-(aminomethyl)anthracene **4**. Samples contained 10 mM sodium phosphate buffer pH 7.0, 38  $\mu\text{M}$  bp of pUC19 plasmid DNA, and 2.5  $\mu\text{M}$  **4** in the presence (circles) and absence (diamonds) of 150 mM NaCl and 260 mM KCl. Prior to photocleavage, the reactions were pre-equilibrated for 1 h in the dark at 22 °C. The samples were then irradiated for 0, 5, 10, 15, 20, 30, 45, or 60 min at 350 nm (22 °C). Cleaved DNA fragments were resolved on a 1.5% nondenaturing agarose gel (Figure S1 in Supporting Information).

While 2.5  $\mu\text{M}$  9-aminomethylanthracene **4** clearly demonstrated time-dependent photoconversion of supercoiled plasmid to its nicked and linear forms (Figure 2; lanes 11–15 vs lanes 3–7 in Figure S1), the addition of 150 mM NaCl and 260 mM KCl markedly enhanced cleavage yields at time points ranging from 15 to 60 min. At  $t = 30$  min of irradiation, the electrophoretic mobilities of the nicked and linear forms of the plasmid began to increase with increasing time (lanes 5–7 in Figure S1). (We presently attribute this effect to photoinduced cross-linking of the anthracene to the DNA.<sup>43,44</sup>) Moreover, the supercoiled plasmid was changed completely into its nicked and linear DNA forms (Figure 2; lanes 5–7 in Figure S1). In the absence of the salts, the highest photocleavage yield to be achieved was 87% of nicked and linear DNA ( $t = 60$  min of  $\text{hv}$ ; Figure 2; lane 15 in Figure S1). The mobilities of the cleaved DNA bands did not appear to change, even after prolonged irradiation times (lanes 9–16 in Figure S1).

The increase in DNA photocleavage produced by the addition of 150 mM NaCl and 260 mM KCl to reactions containing 9-aminomethylanthracene **4** was not anticipated. High concentrations of sodium<sup>+</sup>, potassium<sup>+</sup>, and other cations decrease the association of ligands with double-helical DNA in two ways.<sup>8,26–28</sup> By interacting with the negatively charged phosphate groups in the DNA backbone, counterions can alter DNA structure, e.g., by decreasing minor groove width<sup>33</sup> and helical diameter<sup>32</sup> and by increasing helical twist angle.<sup>30,31</sup> Cations can also effectively compete with positively charged ligands for binding sites on the DNA duplex.<sup>26</sup> As typified by methylene blue<sup>34</sup> (**5** in Figure 1B) and by other ring systems including cyanine dyes,<sup>36</sup> *meso*-substituted porphyrins,<sup>35</sup> and bis-proflavine<sup>37</sup> and 9,10-bis(aminomethyl)anthracene<sup>8</sup> derivatives, the expected effect of a salt-induced reduction in ligand binding is to decrease DNA photocleavage yields.

In order to account for the salt-dependent reactivity of 9-aminomethylanthracene **4**, two initial hypotheses were considered. In the presence of excess amounts of NaCl and KCl, the pyridinylpolyamine side chain of **4** could conceivably form up to three five-membered chelate rings with the alkali metal cations Na<sup>+</sup> and/or K<sup>+</sup>. The change in ligand conformation accompanying complex formation could favor high affinity binding to duplex DNA. Alternatively, the ability of the alkali metal salts to increase DNA photocleavage could arise from a direct interaction between Na<sup>+</sup> and/or K<sup>+</sup> cations and 9-aminomethyl nitrogen lone pair electrons. In 9-aminomethylanthracenes, the nitrogen lone pair quenches the electronically excited state of the anthracene ring by a photoinduced electron transfer mechanism.<sup>45,46</sup> However, the fluorescence quenching can be reversed by coordination of Na<sup>+</sup> or K<sup>+</sup> to the nitrogen atom. The metal–ligand interaction decreases the oxidation potential of the amine. As a result, electron transfer is prevented and the lifetime of the anthracene ring excited state is extended. In the context of our experiments, this would be expected to lead to a Na<sup>+</sup>- or K<sup>+</sup>-induced increase in the production of DNA damaging reactive oxygen species from the photochemically excited singlet or triplet state. In order to test the two hypotheses, DNA photocleavage experiments were repeated utilizing the quaternary amine (9-anthracylmethyl)trimethylammonium chloride (**6** in Scheme 1), a chromophore that is devoid of nitrogen lone pair electrons. The DNA samples were irradiated in the presence and absence of 150 mM NaCl in combination with 260 mM KCl and then electrophoresed. As shown in Figure 1C, a significant salt-induced increase in DNA photocleavage was observed at concentrations of **6** ranging from 10.0 to 1.0 μM (lanes 1–4 vs lanes 8–11 in Figure 1C). This result points to an alternate mechanism in which metal–ligand interactions involving Na<sup>+</sup> or K<sup>+</sup> cations and the amine groups in the side chain of **4** do not play a major role in the salt-induced cleavage enhancement.

Acridine-sensitized one-electron photoreduction of Fe<sup>3+</sup><sup>47</sup> and of Cu<sup>2+</sup><sup>48</sup> results in the production of hydroxyl radicals and/or metal peroxide species that significantly increase levels of oxidative DNA photocleavage.<sup>47–49</sup> In order to minimize interference from redox active metals, all NaCl and KCl solutions used in our experiments were prepared from deionized, distilled water, and 99.999% trace metals basis sodium<sup>+</sup> and potassium<sup>+</sup> chloride salts (Sigma-Aldrich). Notwithstanding, we considered the possibility that the increase in DNA photocleavage generated by the addition of 150 mM NaCl and 260 mM KCl to **4** might be due to contamination of the chloride salt solutions by DNA damaging redox active iron<sup>3+</sup>

and copper<sup>2+</sup> ions. In order to test this hypothesis, photocleavage experiments were conducted in which 10 to 0.5 μM concentrations of 9-aminomethylanthracene **4** were equilibrated with pUC19 plasmid DNA and 150 mM NaCl in combination with 260 mM of KCl, in the presence and absence of a redox active metal salt, either CuCl<sub>2</sub>·2H<sub>2</sub>O or FeCl<sub>3</sub>·6H<sub>2</sub>O. As shown in Figure S2 of the Supporting Information, the addition of the Cu<sup>2+</sup> salt inhibited DNA photocleavage (lanes 1–5 vs lanes 8–12 in Figure S2A), while the Fe<sup>3+</sup> salt had no discernible effect (lanes 1–5 vs lanes 8–12 in Figure S2B). This result indicates that contamination by copper<sup>2+</sup> and/or iron<sup>3+</sup> ions is not the major cause of the chloride salt-induced photocleavage enhancement observed in our experiments.

In order to evaluate the effects of individual chloride salts, pUC19 plasmid DNA was equilibrated with 10.0 to 0.5 μM concentrations of **4** in the presence and absence of either 150 mM NaCl, 260 mM KCl, or 410 mM NaCl. The gel images in Figure S3 show that, when present in combination, 150 mM NaCl and 260 mM KCl (Figure 1A and Figure S3A) produce a much more dramatic enhancement in anthracene-sensitized DNA photocleavage compared to either 150 mM NaCl, 260 mM KCl, or 410 mM NaCl (Figure S3B–D). The addition of the salts altered photocleavage in the following order: 150 mM NaCl and 260 mM KCl (major enhancement, lanes 1–5 vs lanes 8–12 in Figure S3A) > 410 mM NaCl (enhancement, lanes 4 and 5 vs lanes 11 and 12 in Figure S3D), ≈260 mM KCl (enhancement, lanes 1–3 vs lanes 8–10, and inhibition, lane 5 vs lane 12 in Figure S3C) > 150 mM NaCl (minor amounts of photocleavage inhibition, lanes 4 and 5 vs lanes 11 and 12 in Figure S3B). Taken together, the results of these experiments indicate that potassium<sup>+</sup> cations play a more significant role than sodium<sup>+</sup> and chloride<sup>–</sup> anions in the observed photocleavage increase.

**Circular Dichroism Analysis.** Monovalent and divalent cations that bind to nucleic acids bring about a number of changes to the secondary structure of double-helical DNA.<sup>30–33</sup> In particular, the helical twist angle of the duplex is increased, causing the DNA helix to be less tightly wound. This salt-induced alteration in twist angle is characterized by a significant reduction in the positive DNA CD signal at 275 nm,<sup>30,31</sup> making CD a useful tool to monitor helical unwinding. Toward this end, we recorded CD spectra of calf thymus DNA under the conditions of ionic strength employed in the preceding DNA photocleavage experiments (no *hν*; Figure 3). The addition of 150 mM NaCl did not produce a significant change in the overall shape and intensity of the CD spectrum of the CT DNA. Alternatively, the amplitude of the 275 nm band was markedly decreased by 260 mM KCl and by 260 mM KCl in combination with 150 mM NaCl. Taken together with the results of the DNA photocleavage experiments (Figure 1A Figure S3A–C), the CD data suggest that there may be a correlation between salt-induced changes in DNA structure and cleavage yields. The conditions of ionic strength that favor unwinding of the DNA duplex (260 mM KCl alone and in combination with 150 mM NaCl) also increase levels of 9-aminomethylanthracene-sensitized photocleavage. In the absence of KCl, 150 mM NaCl did not have a significant effect (Figure 3 and Figure S3B).

DNA intercalators stack horizontally in between DNA base pairs. Upon binding, the DNA duplex unwinds in order to allow adjacent DNA base pairs to physically separate and make room for the intercalator.<sup>50</sup> As a result, intercalation significantly decreases the intensity of the positive DNA CD signal at 275 nm. (Because anthracene chromophores display relatively

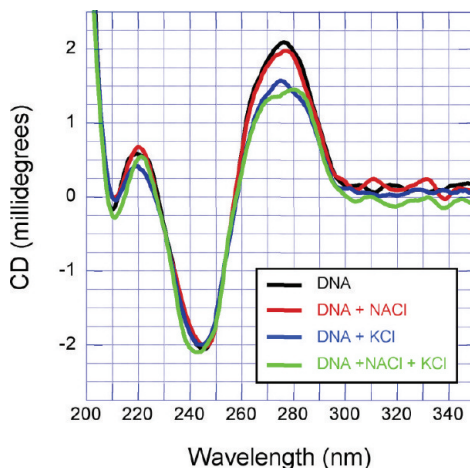


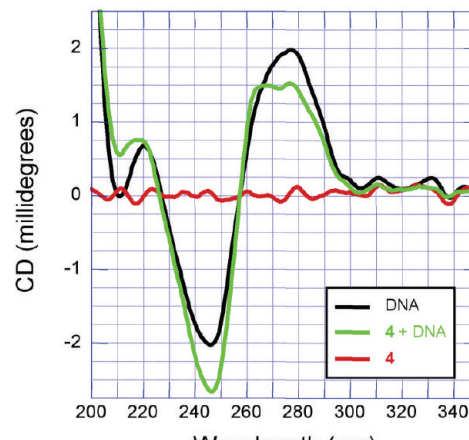
**Figure 3.** CD spectra recorded at 22 °C. Individual samples contained 30  $\mu$ M bp CT DNA and 10 mM sodium phosphate buffer pH 7.0 (black line); 30  $\mu$ M bp CT DNA, 10 mM sodium phosphate buffer pH 7.0, and 150 mM NaCl (red line); 30  $\mu$ M bp CT DNA, 10 mM sodium phosphate buffer pH 7.0, and 260 mM KCl (blue line); 30  $\mu$ M bp CT DNA, 10 mM sodium phosphate buffer pH 7.0, and 150 mM NaCl, and 260 mM KCl (green line). Prior to recording the spectra, the samples were pre-equilibrated for 1 h in the dark at 22 °C.

weak absorption at this wavelength, the DNA CD signal at 275 nm has been used as a sensitive probe for intercalative binding by anthracene derivatives.<sup>51</sup> Toward this end, we recorded the CD spectra of a series of solutions containing CT DNA and/or 10.0  $\mu$ M of **4** in the presence and absence of 150 mM NaCl in combination with 260 mM KCl (Figure 4). Under the low ionic strength conditions, the addition of compound **4** caused the CT DNA CD signal at 275 nm to decrease in intensity (Figure 4A). It can therefore be inferred from the CD spectra that 9-aminomethylanthracene derivative **4** may be engaging in DNA intercalation.<sup>51</sup> Alternatively, there were no anthracene-induced variations in the CT DNA CD signal when 150 mM NaCl and 260 mM KCl were present (Figure 4B). Because 10.0  $\mu$ M anthracene produced significant photodegradation of plasmid DNA under equivalent conditions of ionic strength (150 mM NaCl in combination with 260 mM KCl), the data suggest that **4** is interacting with DNA by a nonintercalative binding mode that does not make substantial changes to DNA secondary structure.

#### Absorption Titration and Induced Circular Dichroism

**Data.** UV-vis spectrophotometry was utilized in order to further study anthracene/DNA interactions. Our first DNA titration experiment was conducted in the absence of 150 mM NaCl and 260 mM KCl. Small volumes of CT DNA were sequentially added to a solution containing 50  $\mu$ M **4** (Figure 5A). An isosbestic point at 393 nm was observed, indicating that the titration produced a transition between two spectroscopically distinct anthracene species. Notably, saturating amounts of CT DNA (250  $\mu$ M bp and 300  $\mu$ M bp) induced significant hypochromicity and a significant bathochromic shift in the peak positions of the anthryl vibronic absorption bands. These spectral features are hallmarks of anthracene intercalation<sup>8,9,51,52</sup> and are consistent with the decrease in the 275 nm CT DNA CD signal that compound **4** produces in the absence of NaCl and KCl (Figure 4A). Thus, one of the two spectroscopic species revealed by the absorption titration spectra may arise from intercalative binding of the anthracene chromophore to the DNA.

#### A) no salts



#### B) 150 mM NaCl + 260 mM KCl

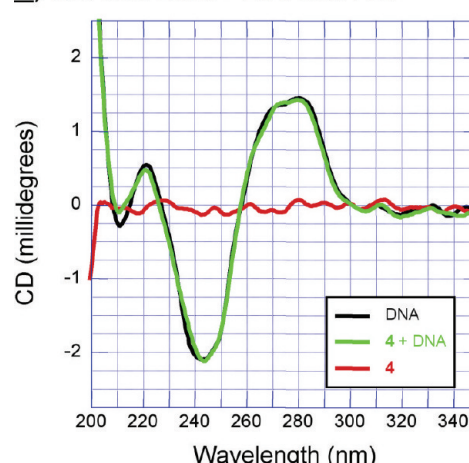


**Figure 4.** CD spectra recorded at 22 °C (A) in the absence of 150 mM NaCl and 260 mM KCl and (B) in the presence of 150 mM NaCl and 260 mM KCl. Individual samples contained 30  $\mu$ M bp CT DNA and 10 mM sodium phosphate buffer pH 7.0 (black line); 10  $\mu$ M of **4**, 30  $\mu$ M bp CT DNA, and 10 mM sodium phosphate buffer pH 7.0 (green line); and 10  $\mu$ M of **4** and 10 mM sodium phosphate buffer pH 7.0 (red line). Prior to recording the spectra, the samples were pre-equilibrated for 1 h in the dark at 22 °C.

In a second titration experiment, CT DNA was added to 9-aminomethylanthracene **4** in the presence of 150 mM NaCl and 260 mM KCl. In contrast to the data shown in Figure 5A, the wavelengths and intensities of the three most prominent anthryl vibronic absorption maxima were not appreciably altered (Figure 5B). This result suggests that 9-aminomethylanthracene **4** is no longer engaging in intercalation. In the case of intercalative DNA binding, the strong hypochromism and red-shifts in the absorption spectrum of the chromophore are produced by electronic effects involving  $\pi$ - $\pi$  stacking and dipole-dipole interactions with DNA base pairs. The strength of these electronic interactions is inversely proportional to the cube of the distance separating the chromophore and the bases.<sup>53</sup> Thus, when compared to intercalation, the absorption spectra of groove-binding anthracene derivatives show minimal if any red-shifting and intermediate amounts of hypochromism.<sup>8,9,52</sup>

Self-stacking of aromatic chromophores in aqueous solution can lead to the formation of dimers and higher order

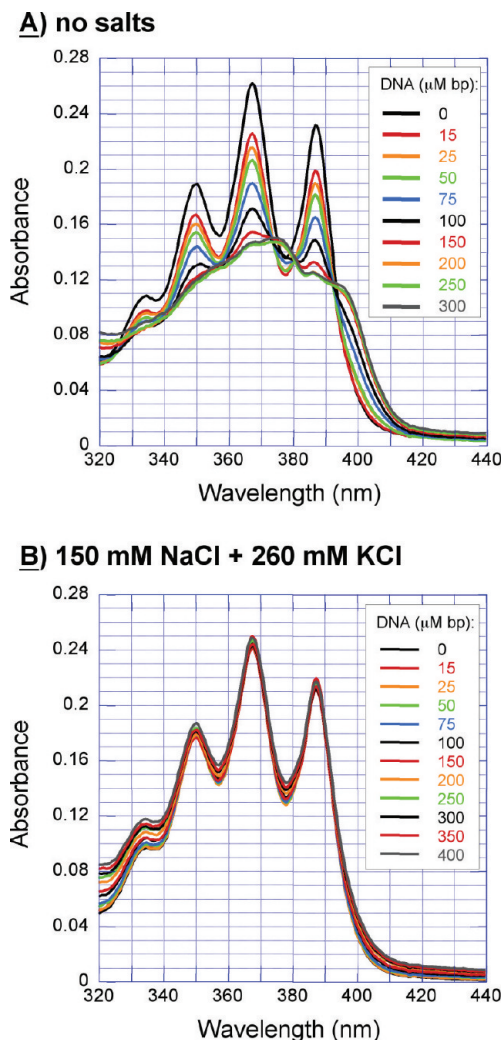


**Figure 5.** UV–vis absorption titration spectra of 50  $\mu\text{M}$  of 4 recorded at 22  $^{\circ}\text{C}$  (A) in the absence of 150 mM NaCl and 260 mM KCl and (B) in the presence of 150 mM NaCl and 260 mM KCl. Individual samples contain 10 mM sodium phosphate buffer pH 7.0 and increasing concentrations of CT DNA (0  $\mu\text{M}$  bp to 300  $\mu\text{M}$  bp or 400  $\mu\text{M}$  bp). Following each sequential DNA addition, the solution was allowed to equilibrate for 1 h in the dark before the UV–vis spectrum was recorded. All absorption spectra have been corrected for sample dilution.

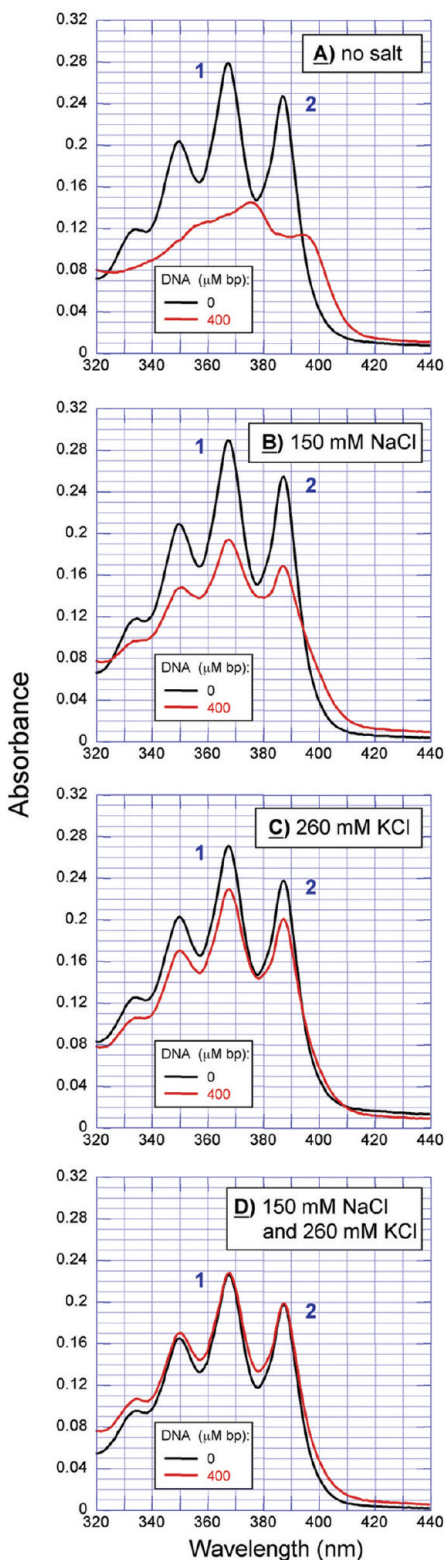
aggregates.<sup>54,55</sup> In general, the absorption of the aggregate is hypochromic with respect to the absorption of the corresponding monomer. Taking this into account, we considered a scenario in which chromophore self-stacking in the absence of DNA might produce hypochromicity in the absorption spectrum of compound 4 (0  $\mu\text{M}$  bp DNA; Figure 5B). This interaction could then conceal changes in chromicity caused by subsequent DNA binding. In order to investigate this possibility, UV–vis spectra of a solution containing 50  $\mu\text{M}$  4, 150 mM NaCl, and 260 mM KCl (no DNA) were recorded in the presence of 0% (v/v) to 10% (v/v) concentrations of dimethyl sulfoxide, a reagent that is routinely used to disrupt intermolecular stacking of aromatic chromophores<sup>56</sup> (Figure S4 in the Supporting Information). Upon the addition of the DMSO, anthryl chromicity was unchanged, indicating that compound 4 was not self-stacking under the experimental conditions employed in the preceding DNA titration experiment (Figure 5B). It is therefore reasonable to hypothesize that

when compound 4 is in the presence of 150 mM NaCl and 260 mM KCl, its anthryl ring is associated with DNA by an external interaction. At a significant distance from the chromophore, the DNA base pairs would be expected to have minimal influence on anthracene absorption (Figure 5B).

In order to study of effects of individual salts on absorption spectra, 50  $\mu\text{M}$  compound 4 was equilibrated with saturating amounts of DNA in the presence of 150 mM NaCl, 260 mM KCl, or 150 mM NaCl and 260 mM of KCl (Figure S5 of Supporting Information). The intensities of the vibronic bands of 4 were found to decrease according to salt conditions in the following order: 150 mM NaCl and 260 mM of KCl > 260 mM of KCl > 150 NaCl. This trend is in good general agreement with the relative levels of DNA photocleavage produced in the presence of equivalent concentrations of the chloride salts: 150 mM NaCl and 260 mM KCl (large salt-induced DNA photocleavage enhancement observed) > 260 mM KCl (intermediate enhancement) > 150 mM NaCl (minor amount of DNA photocleavage cleavage inhibition observed) (Figure S3 in the Supporting Information). Because the strength of  $\pi$ – $\pi$  stacking and dipole–dipole electronic interactions with DNA is proportional to anthracene hypochromicity and is inversely proportional to separation between the DNA base pairs and the chromophore,<sup>53</sup> the ability of compound 4 to photocleave DNA may increase as a function of increasing distance from the DNA bases.

In Figure 6 are the complete set of UV–vis absorption spectra of 50  $\mu\text{M}$  4 before and after the addition of saturating amounts of CT DNA (400  $\mu\text{M}$  bp). In the absence of the chloride salts, the DNA produced strong hypochromicity accompanied by respective 8 and 7 nm red-shifts in the 0–1 and 0–0 vibronic bands of 4, spectral features that are characteristic of anthracene intercalation (Figure 6A).<sup>9,51</sup> In the presence of the individual salts, either 150 mM NaCl (Figure 6B) or 260 mM KCl (Figure 6C), evidence of groove binding was indicated by intermediate hypochromicity and minimal bathochromicity,<sup>8,9,52</sup> with a significantly more pronounced effect being exhibited by 150 mM NaCl. In the case of the combination of salts (150 mM NaCl and 260 mM KCl), the vibronic absorption maxima of the two spectra were nearly superimposable (Figure 6D), consistent with our hypothesis that compound 4 is associated with the DNA helix through a mode in which the anthracene ring of the chromophore is external to the DNA base pairs.

In order to corroborate the absorption data shown in Figure 6, we recorded induced circular dichroism spectra of 50  $\mu\text{M}$  4 equilibrated with CT DNA (150  $\mu\text{M}$  bp). In the absence of the chloride salts, we observed positive ICD bands with peak positions closely resembling the red-shifted vibronic bands in the absorption spectrum of DNA-bound 4 (Figure 6A; Figure S6 of Supporting Information). This ICD signature is typical of 9-aminomethylanthracene derivatives and is thought to arise from an intercalative binding mode in which the long axis of the anthracene is perpendicular to the long axis of the DNA base pairs.<sup>8,9,19,51,52</sup> The addition of 150 mM NaCl and 260 mM KCl to the anthracene solutions caused the ICD signal of DNA-bound 4 to become significantly attenuated (Figure S6). In general, a major reduction in ICD signal intensity is displayed when anthracene chromophores undergo a change in binding from intercalation to a nonintercalative mode (e.g., groove binding).<sup>8,9</sup> Furthermore, the ICD peak positions of 4 were found to be dissimilar to the anthryl vibrational bands of the corresponding absorption spectrum recorded in the presence of the chloride salts (Figures S6 and 6D). This suggests that the

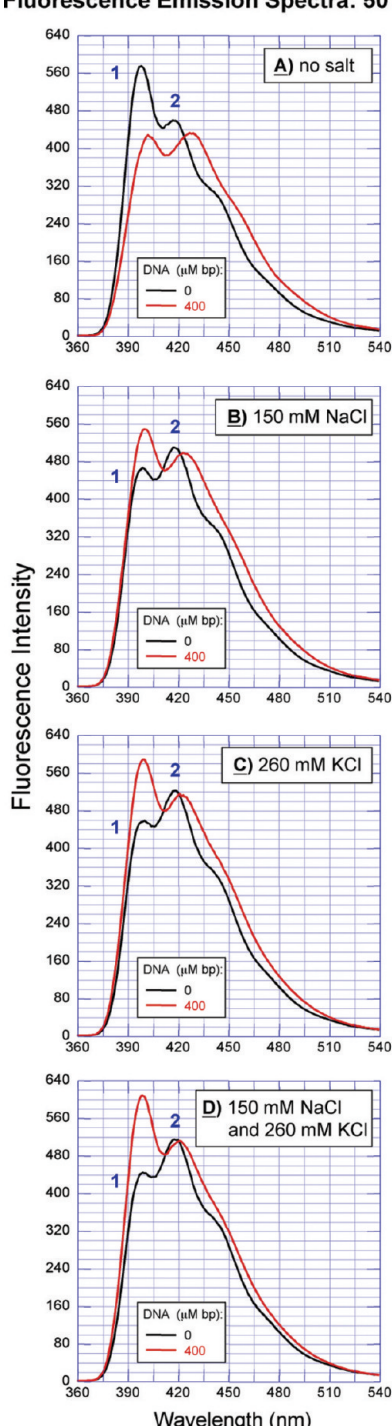
Absorption Spectra: 50  $\mu$ M 4 vs. DNA

**Figure 6.** UV-vis absorption spectra of 50  $\mu$ M 4 equilibrated in the absence (black line) and presence (red line) of 400  $\mu$ M bp CT DNA (10 mM sodium phosphate buffer, pH 7.0): (A) no salt,  $\Delta\lambda_{\max 1} = 8$  nm,  $\Delta\lambda_{\max 2} = 7$  nm; (B) 150 mM NaCl,  $\Delta\lambda_{\max 1} = 0$  nm,  $\Delta\lambda_{\max 2} = -0.5$  nm; (C) 260 mM KCl,  $\Delta\lambda_{\max 1} = 0.5$  nm,  $\Delta\lambda_{\max 2} = 0$  nm; (D) 150 mM NaCl and 260 mM KCl,  $\Delta\lambda_{\max 1} = 0$  nm,  $\Delta\lambda_{\max 2} = 0$  nm. Note: Peak 1 = 0-1 transition; peak 2 = 0-0 transition;  $\Delta\lambda_{\max n} = (\lambda_{\max} \text{ of peak } n \text{ in the presence of DNA} - \lambda_{\max} \text{ of peak } n \text{ in the absence of DNA})$ .

ICD spectra may arise from a secondary binding interaction<sup>9</sup> (e.g., residual intercalation) that is unrelated to the principal, nonintercalative binding mode indicated by the absorption data (Figures S6 and 6D). Notwithstanding, the absorption and ICD data support the hypothesis that the addition of the chloride salts to the DNA solution disrupts the intercalative binding of compound 4.<sup>9</sup>

**Fluorescence Spectroscopy.** DNA intercalation of 9-aminomethylanthracene derivatives results in strong fluorescence quenching of the anthryl fluorophore's vibronic emission bands.<sup>8,19,52,57</sup> In some cases, this is accompanied by a change in relative band intensities<sup>19,57</sup> and in red-shifting of their peak positions.<sup>8,57</sup> The quenching produced by intercalation is dependent on DNA sequence in the following order: d(GC) > CT DNA  $\gg$  d(AT)  $\gg$  d(A)-d(T).<sup>57</sup> Because the oxidation potential of guanine is the lowest of the four DNA bases, it has been suggested that an electron transfer pathway is responsible.<sup>19</sup> (The singlet energies of the DNA bases are significantly higher than that of anthracene, making energy transfer to DNA an unlikely alternative.<sup>19,57</sup>) Upon switching a DNA-bound anthracene from an intercalative to a groove-binding mode, the fluorescence quenching can be partially reversed.<sup>8</sup> In the case of electrostatic interaction of anthracenes with anionic media (e.g., poly(sodium 4-styrenesulfonate) and sodium dodecyl sulfate), an increase (rather than decrease) in anthryl emission intensity is observed.<sup>57</sup> Thus, in order to obtain additional insights into the nature of the interactions of 9-aminomethylanthracene 4 with DNA, we recorded a complete set of fluorescence emission spectra before and after the addition of saturating amounts of CT DNA (Figure 7; 50  $\mu$ M 4, 400  $\mu$ M bp CT DNA; 150 mM NaCl, and/or 260 mM KCl). The samples were excited at 393 nm, a wavelength at which absorbance was found to be relatively independent of DNA concentration and ionic strength (Figure 6). In the absence of the chloride salts, the addition of the CT DNA produced significant fluorescence quenching and red-shifting of the anthryl vibronic bands, consistent with intercalative binding (Figure 7A). As the chloride salt concentration was increased up to 150 mM NaCl and 260 mM KCl, the CT DNA caused a progressive reduction in (i) red-shifting of the emission spectra and (ii) quenching of the low-energy 0-1 and, to a greater extent, the high-energy 0-0 anthryl bands (peaks 2 and 1 in Figure 7). The latter changes in relative peak intensity may arise from differences in the equilibrium geometries of the ground states and excited vibronic states of the free vs DNA-bound anthracene.<sup>19</sup> Notwithstanding, a considerable increase in anthryl fluorescence emission intensity was produced by the addition of the CT DNA to the solution containing the combination of chloride salts (150 mM NaCl and 260 mM KCl; Figure 7D). This result points to a nonintercalative interaction<sup>57</sup> between compound 4 and the CT DNA. The ability of the chloride salts to induce significant spectral changes to the emission spectrum of free 4 (no CT DNA) is consistent with literature reports in which metal chelating 9-aminomethylanthracene fluorophores have been used to detect  $\text{Na}^+$  and  $\text{K}^+$  cations in aqueous and nonaqueous media<sup>45,46</sup> (Figures 7B-D vs Figure 7A).

**Thermal Melting of DNA.** Ligands that preferentially interact with double-helical DNA stabilize the nucleic acid duplex and, as a result, increase the helical melting temperature. Alternatively, preferred association with single-stranded DNA can lead to duplex destabilization and a concomitant reduction in  $T_m$ .<sup>58</sup> In this regard, DNA melting temperature trends can reveal important information regarding the effects of ligand

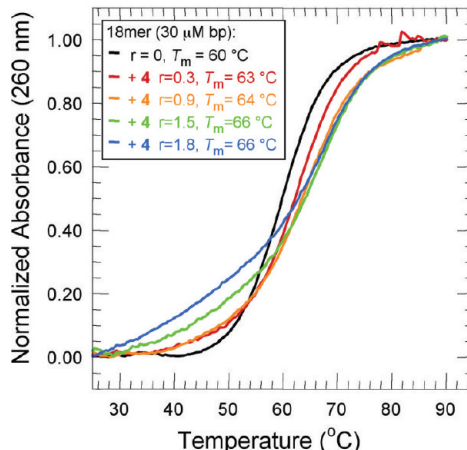
Fluorescence Emission Spectra: 50  $\mu$ M 4 vs. DNA

**Figure 7.** Fluorescence emission spectra with excitation at 393 nm of 50  $\mu$ M 4 equilibrated in the absence (black line) and presence (red line) of 400  $\mu$ M bp CT DNA (10 mM sodium phosphate buffer, pH 7.0): (A) no salt,  $\Delta\lambda_{\text{max}1} = 4$  nm,  $\Delta\lambda_{\text{max}2} = 10$  nm; (B) 150 mM NaCl,  $\Delta\lambda_{\text{max}1} = 1$  nm,  $\Delta\lambda_{\text{max}2} = 6$  nm; (C) 260 mM KCl,  $\Delta\lambda_{\text{max}1} = 0$  nm,  $\Delta\lambda_{\text{max}2} = 2$  nm; (D) 150 mM NaCl and 260 mM KCl,  $\Delta\lambda_{\text{max}1} = 0$  nm,  $\Delta\lambda_{\text{max}2} = 3$  nm. Note: peak 1 = 0–0 transition; peak 2 = 0–1 transition;  $\Delta\lambda_{\text{max}n} = (\lambda_{\text{max}} \text{ of peak } n \text{ in the presence of DNA} - \lambda_{\text{max}} \text{ of peak } n \text{ in the absence of DNA})$ .

interactions on the dynamics of DNA structure. In our first set of thermal melting experiments, DNA isotherms were recorded in the absence and presence of 150 mM NaCl and 260 mM KCl, at dye to DNA bp molar ratio values ( $r$ ) ranging from

0 to 2.4 (Figure 8). The 18-mer hairpin duplex sequence 5'-CACTGGTCTCTACCAGTG-3' was used as an alternative

## A) 18 mer DNA, no salts



## B) 18 mer DNA, 150 mM NaCl + 260 mM KCl

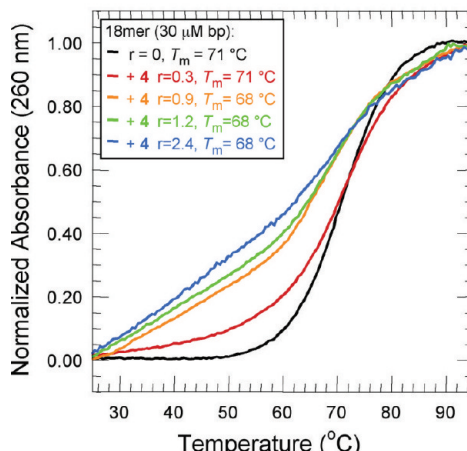


**Figure 8.** Normalized melting isotherms of 30  $\mu$ M bp of 18-mer hairpin duplex 5'-CACTGGTCTCTACCAGTG-3' in 10 mM sodium phosphate buffer, pH 7.0, without and with compound 4. Melting curves were recorded (A) in the absence of 150 mM NaCl and 260 mM KCl ( $r = 0$  to 1.8) and (B) in the presence of 150 mM NaCl and 260 mM KCl ( $r = 0$  to 2.4). Abbreviation:  $r = [\text{dye}] / [\text{DNA bp}]$ .

to calf thymus DNA, in order to avoid exceeding the maximum recordable temperature of our instrumentation (95 °C) when working under high chloride salt concentrations. Shown in Figure 8A are the normalized melting curves generated in the absence of NaCl and KCl. (Representative, un-normalized and first-derivative melting curves are in Figure S7A of Supporting Information.) Under these conditions, the  $T_m$  value obtained for the 18-mer hairpin duplex was 60 °C. Upon the addition of 9-aminomethylanthracene derivative 4, the  $T_m$  was increased to a maximum of 66 °C at DNA saturation ( $r \geq 1.5$ ). Intercalative binding of anthracene chromophores enhances duplex stability and substantially increases DNA melting temperature.<sup>8,9,19,52</sup> In the case of groove-binding anthracenes, changes in melting temperature are generally not observed.<sup>9</sup> Thus, in the absence of salts, the high  $T_m$  values produced by compound 4 are consistent with intercalative binding. Interestingly, the increase in melting temperature at each  $r$  value was accompanied by a

progressive broadening of the 18-mer hairpin duplex melting curve (Figure 8A).

In our next experiment, melting curves of the 18-mer hairpin duplex were recorded in the presence of 150 mM NaCl in combination with 260 mM KCl (Figure 8B and Figure S7B). The inclusion of the chloride salts raised the  $T_m$  value of the duplex from 60 °C ( $r = 0$  in Figure 8A) to 71 °C ( $r = 0$  in Figure 8B). Compound 4 was then added at  $r$  values of 0.3 up to 2.4. This resulted in an additional, progressive broadening of the DNA melting curves accompanied by an incremental shift of each curve to a lower temperature range. At DNA saturation ( $r \geq 0.9$ ), the melting temperature of the duplex was reduced from 71 to 68 °C.

The majority of DNA ligands increase, rather than decrease, the  $T_m$  of double-helical DNA.<sup>58</sup> Therefore, in order to confirm the preceding results, an additional set of melting isotherms was obtained using sonicated CT DNA. In the absence of the chloride salts, compound 4 ( $r = 0.3$  in Figure 9A), and a positive control, the classical intercalating dye methylene blue

(5;  $r = 0.3$  in Figure 9B), each raised the  $T_m$  value of the duplex DNA from 68 to 75 °C, with the isotherm of 4 melting over a broader range than the isotherm of 5 (Figure 9). We then recorded a complete set of thermal melting curves in which CT DNA was pre-equilibrated with compound 4 at  $r$  values of 0 to 1.2 (no chloride salts; Figure S8 of Supporting Information). The magnitude of the  $\Delta T_m$  value obtained at DNA saturation (12 °C;  $r \geq 1.0$ ) is characteristic of intercalative binding of anthracene derivatives to DNA.<sup>8,9,19,52</sup>

Individual chloride salts, either 150 mM NaCl or 150 mM KCl, were then added to DNA solutions. The  $T_m$  value of the calf thymus DNA was raised from 68 to 85 °C and 88 °C by NaCl and KCl, respectively ( $r = 0$  in Figure 9). The inclusion of the methylene blue (5) did not significantly alter the CT DNA melting curves ( $r = 0.3$  in Figure 9B). In contrast, 9-aminomethylanthracene 4 broadened and shifted the melting curves to a lower temperature range ( $r = 0.3$  in Figure 9A). In the case of 150 mM NaCl, the 85 °C melting temperature was not changed. Alternatively, when 150 mM KCl was present, compound 4 lowered the  $T_m$  of the CT DNA from 88 to 86 °C ( $r = 0.3$  in Figure 9A).

Taken together, the 18-mer hairpin duplex and CT DNA data support our hypothesis that compound 4 engages in DNA intercalation under conditions of low ionic strength (Figures 8A and 9A; Figure S9). In DNA samples containing high concentrations of KCl, alone and in combination with NaCl, the addition of 4 to DNA decreases  $T_m$ . These findings suggest that intercalation has been disrupted in favor of a binding mode that does not confer appreciable stabilization onto the DNA duplex (Figures 8B and 9A). The majority of ligands that lower DNA melting temperature are metal salts or compounds that form destabilizing adducts with DNA bases.<sup>59–61</sup> Interactions between anthracenes and DNA are primarily noncovalent in nature.<sup>43,44</sup> Although long wave UV irradiation of anthracene–DNA complexes can initiate covalent binding of the hydrocarbon to DNA bases, precautions were taken to protect our melting temperature samples from prolonged exposure to light. Therefore, the question remains as to why, under conditions of high ionic strength, compound 4 appears to exert a destabilizing effect that reduces DNA melting temperature. In the presence of anthracene derivative 4, the DNA melting curves also exhibited a significant degree of transition broadening (Figures 8 and 9A; Figure S8). This phenomenon normally occurs when a given ligand stabilizes (or destabilizes) specific regions or sequences within a DNA duplex to a greater degree than other regions.<sup>58</sup>

#### Chemically Induced Changes in DNA Photocleavage.

As a test for reactive oxygen species, we used the singlet oxygen ( ${}^1\text{O}_2$ ) scavenger sodium azide and the hydroxyl radical ( $\cdot\text{OH}$ ) scavengers sodium benzoate and D-mannitol. Individual samples contained pUC19 plasmid DNA and 9-aminomethylanthracene derivative 4 in the presence and absence of 150 mM NaCl in combination with 260 mM KCl. The percent of total photocleavage inhibited by each of the scavengers is shown in Table 1. Sodium azide, sodium benzoate, and D-mannitol produced a considerable inhibitory effect, indicating that singlet oxygen and hydroxyl radicals contribute to DNA photocleavage. Moreover, higher levels of photocleavage inhibition occurred in the reactions containing the combination of chloride salts. The most significant result was produced by sodium azide. Using this  ${}^1\text{O}_2$  scavenger, yields of DNA photocleavage were respectively reduced by  $83 \pm 6\%$  and by  $27 \pm 1\%$  in the presence and absence of 150 mM NaCl and 260 mM

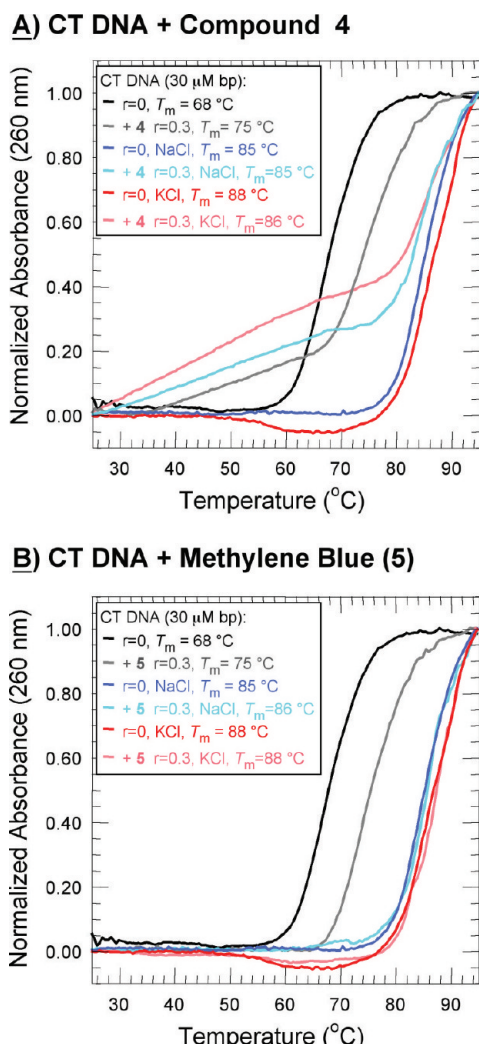


**Figure 9.** Normalized melting isotherms of 30  $\mu\text{M}$  bp of CT DNA in 10 mM sodium phosphate buffer, pH 7.0: without chloride salts (black/gray lines), with 150 mM NaCl (blue/cyan lines), or with 150 mM KCl (red/pink lines). Melting curves were recorded in the absence ( $r = 0$ ; dark lines) and presence ( $r = 0.3$ ; light lines) of (A) 10  $\mu\text{M}$  compound 4 and (B) 10  $\mu\text{M}$  methylene blue (5). Abbreviation:  $r = [\text{dye}]/[\text{DNA bp}]$ .

**Table 1. Average % Inhibition of DNA Photocleavage by ROS Scavengers<sup>a</sup>**

scavenger	ROS	% inhibition, no salt	% inhibition, salt
sodium azide	$^1\text{O}_2$	27 ± 1	83 ± 6
sodium benzoate	$\cdot\text{OH}$	21 ± 5	55 ± 7
D-mannitol	$\cdot\text{OH}$	2 ± 1	17 ± 4

<sup>a</sup>Photocleavage inhibition reactions consisted of 38  $\mu\text{M}$  bp of pUC19 plasmid DNA equilibrated with 2.5  $\mu\text{M}$  4, 100 mM scavenger, and 10 mM sodium phosphate buffer pH 7.0, in the absence and presence of 150 mM NaCl in combination with 260 mM KCl. Samples were aerobically irradiated for 60 min at 350 nm. Percent inhibition data were averaged over three to four trials with error reported as standard deviation.

KCl (Table 1). These data suggest that there is a sharp increase in the production of singlet oxygen under conditions of high ionic strength. The salt-dependent involvement of singlet oxygen was then confirmed using deuterium oxide, a solvent that increases the lifetime of  $^1\text{O}_2$  (Figure S9 in Supporting Information).<sup>62</sup> In the presence of the combination of chloride salts, the average percent yields of DNA photocleavage increased from 67 ± 10% in ddH<sub>2</sub>O to 100 ± 0% in D<sub>2</sub>O. In contrast, deuterium oxide had little effect in the absence of the chloride salts, where the average yields of cleaved DNA were 42 ± 2% and 40 ± 2% in ddH<sub>2</sub>O and D<sub>2</sub>O, respectively (Figure S9).

In a study of DNA photocleavage by cyanine dyes, Åckerman and Tuite found that externally bound cyanines produced more DNA photocleavage than when the same dyes were engaged in DNA intercalation.<sup>36</sup> Scavenger experiments showed that, when bound externally, the cyanine dyes generated DNA cleavage by photosensitizing the production of singlet oxygen. However, when the dyes were intercalated, there was no evidence of the involvement of singlet or ground state triplet oxygen in the photocleavage reactions. This finding was considered to be consistent with a general phenomenon in which the microenvironment of the DNA intercalation pocket prevents fluorescent dyes from freely interacting with ground state triplet oxygen and other quenching agents.<sup>36,63</sup> The same principle may be used to explain why levels of DNA photocleavage are increased when the combination of 150 mM NaCl and 260 mM KCl is added to 9-aminomethylanthracene 4. The presence of the chloride salts appears to trigger a change in anthracene binding from intercalation to an external mode in which the anthracene chromophore may be considerably more accessible to dissolved oxygen. This in turn may lead to an increase the anthracene-sensitized production of DNA damaging singlet oxygen and hydroxyl radicals.

**Summary and General Discussion.** In this paper, we describe the synthesis and DNA interactions of a new 9-aminomethylanthracene dye N-substituted with a pyridinylpolyamine side chain (4 in Scheme 1). We found that the levels of DNA photocleavage produced by compound 4 were enhanced when 150 mM NaCl and 260 mM KCl were added to cleavage reactions (0.5–10  $\mu\text{M}$  4, 350 nm, pH 7.0, 22 °C; Figures 1A and 2; Figures S1 and S3A). This finding was quite unexpected. Because conditions of high ionic strength typically decrease the association of DNA photosensitizers and other ligands with double-helical DNA, it is anticipated that photocleavage yields will be substantially decreased (Figure 1B).<sup>8,27,28,34–37</sup> Therefore, a major goal of the research described in this paper was to determine why DNA photocleavage was enhanced upon the addition of 150 mM NaCl and 260 mM KCl to

9-aminomethylanthracene 4 cleavage reactions. In preliminary experiments, the inclusion of micromolar concentrations of CuCl<sub>2</sub>·2H<sub>2</sub>O or FeCl<sub>3</sub>·6H<sub>2</sub>O in chloride salt solutions did not add to photocleavage yields, ruling against contamination by redox active Cu<sup>2+</sup> and Fe<sup>3+</sup> ions (Figure S2). Alternatively, DNA photocleavage was enhanced upon the addition of 150 and 260 mM KCl to the quaternary amine (9-anthracenylmethyl)trimethylammonium chloride (6) (Figure 1C), ruling out a major involvement of the amine group lone pair electrons in the side chain of 4. When the chloride salts were tested in combination and individually, the largest photocleavage enhancement was produced by 150 mM NaCl in combination with 260 mM KCl, followed by 410 mM NaCl and 260 mM KCl (Figure 1 and Figure S3). Thus, potassium<sup>+</sup> cations were shown to play a significant role. A correlation between K<sup>+</sup>-induced helical unwinding and an increase in cleavage yields was then indicated by CD spectrometry (Figure 3).

Our next experiments were focused on determining if the salt-induced increase in DNA photocleavage was related to a change in anthracene binding mode. In the absence of the chloride salts, intercalative binding of 4 was indicated by the following lines of evidence. The addition of 4 to CT DNA caused the DNA CD signal at 275 nm to decrease in intensity (Figure 4A).<sup>51</sup> The addition of CT DNA to 4 produced (i) significant hypochromicity and bathochromicity in the anthracene's vibronic absorption bands (Figures 5A and 6A),<sup>9,51</sup> (ii) a relatively strong, corresponding, positive induced CD signal (Figure S6),<sup>8,9,19,51,52</sup> and (iii) significant fluorescence quenching and red-shifting of the anthryl vibronic emission spectrum (Figure 7A).<sup>19,57</sup> Finally, compound 4 at DNA saturation produced helical stabilization that was associated with a significant increase in the  $T_m$  values of an 18-mer hairpin duplex (Figure 8A) and calf thymus DNA (Figure S8).<sup>8,9,19,52</sup>

Evidence obtained in the presence of the combination of chloride salts (150 mM NaCl and 260 mM KCl) pointed to a nonintercalative binding mode. The addition of 4 to CT DNA did not alter the intensity of the DNA CD signal at 275 nm (Figure 4B). The addition of CT DNA to 4 produced (i) minimal changes to the wavelengths and intensities of the major anthryl vibronic band absorption maxima (Figures 5B and 6D), (ii) a very weak, positive induced CD signal (Figure S6),<sup>8,9</sup> and (iii) enhanced fluorescence emission accompanied by minimal red-shifting of the anthryl vibronic peak positions (Figure 7D).<sup>57</sup> Lastly, compound 4 at DNA saturation shifted the melting curves of DNA to a lower temperature range, generating a decrease in the  $T_m$  of the 18-mer hairpin duplex consistent with helical destabilization (Figure 8B).<sup>58</sup> The addition of 4 to solutions containing the individual salts (either 150 mM NaCl or 150 mM KCl) also shifted the melting curves of CT DNA to lower temperatures (Figure 9A). This effect was more pronounced in the case of 150 mM KCl, where compound 4 exhibited a destabilizing effect that lowered  $T_m$  (Figure 9A).

All in all, the preceding data indicate that the increase in anthracene-sensitized photocleavage that is produced by the addition of 150 mM NaCl and 260 mM KCl to the DNA reactions is likely to be accompanied by a salt-induced change in anthracene binding from intercalation to a nonintercalative mode. While unraveling the precise nature of the interactions between DNA and compound 4 will rest on high-resolution structural analyses, the evidence presented in this paper points to external binding. In the presence of the chloride salts, the addition of saturating amounts of CT DNA does not alter the

positions and intensities of the major vibronic absorption maxima of **4**, indicating that there is a significant distance separating the anthracene chromophore from the DNA base pairs. Secondly, the sharp increase in singlet oxygen production that occurs under conditions of high ionic strength is consistent with a binding mode in which the anthracene chromophore is relatively accessible to ground state triplet oxygen.<sup>36,63</sup>

## CONCLUSIONS

Within the cell nucleus where genomic DNA is contained, average concentrations of NaCl and KCl are ~150 and 260 mM, respectively.<sup>22–25</sup> Thus, in photodynamic cancer therapy, an ideal DNA photosensitizer should function optimally under conditions of high ionic strength. Toward this end, we have shown that the addition of 150 mM NaCl and 260 mM KCl to 9-aminomethylanthracene **4** reactions produces a significant and unexpected increase in anthracene-sensitized DNA photocleavage (350 nm, pH 7.0). In the presence of micromolar concentrations of **4**, the combination of chloride salts triggers the photodegradation of supercoiled, nicked, and linear forms of pUC19 plasmid into a diffuse band of high mobility DNA fragments (lanes 1–3 vs lanes 8–10 in Figure 1A). Our data point to a salt-induced change in DNA binding mode from intercalation to an external interaction that efficiently promotes the formation of reactive oxygen species. Helical unwinding by monovalent potassium cations may play an important role in this process. We envisage that the insights gained from this research will contribute to the development of new and structurally diverse phototherapeutic agents that function optimally in the ionic environment of the cell nucleus.

## ASSOCIATED CONTENT

### Supporting Information

Figure S1, agarose gel showing time-dependent photocleavage of pUC19 plasmid by N-substituted 9-(aminomethyl)-anthracene **4**; Figure S2, agarose gels showing photocleavage of pUC19 plasmid by **4** in the presence and absence of (A) CuCl<sub>2</sub>·2H<sub>2</sub>O and (B) FeCl<sub>3</sub>·6H<sub>2</sub>O; S2 discussion; Figure S3, agarose gels showing photocleavage of pUC19 plasmid by **4** in the presence and absence of (A) 150 mM NaCl and 260 mM KCl, (B) 150 mM NaCl, (C) 260 mM KCl, and (D) 410 mM NaCl; Figure S4, UV-vis absorption titration spectra of **4** with 150 mM NaCl and 260 mM KCl in the presence of increasing concentrations of DMSO; Figure S5, UV-vis absorption spectra of **4** with CT DNA in the presence of 150 mM NaCl in combination with 260 mM KCl, 260 mM KCl, or 150 mM NaCl; Figure S6, double y-axis plot of (A) ICD spectra and (B) UV-vis absorption spectra of **4** and/or CT DNA; Figure S7, un-normalized and corresponding first derivative melting isotherms an 18-mer hairpin duplex in the absence and presence of **4** (*r* = 0 and 0.3); Figure S8, normalized thermal melting curves of CT DNA in the absence and presence of **4** (*r* = 0–1.2). Figure S9, agarose gels showing photocleavage of pUC19 plasmid by **4** in the presence of ddH<sub>2</sub>O or D<sub>2</sub>O. This material is available free of charge via the Internet at <http://pubs.acs.org>.

## AUTHOR INFORMATION

### Corresponding Author

\*Phone +34 91 8854691, Fax +34 91 8854686, e-mail antonio.lorente@uah.es (A.L.). Phone +1 (404) 413-5522, Fax +1 (404) 413-5505, e-mail kbgrant@gsu.edu (K.B.G.).

## Funding

This work was supported by the CAM-UAH (CCG10-UAH/PPQ-5961, M.-J.F.) and by the National Science Foundation (CHE-0718634, K.B.G.).

## ACKNOWLEDGMENTS

We thank Georgia State University Professors Dabney W. Dixon, Donald Hamelberg, and W. David Wilson for helpful discussions.

## ABBREVIATIONS

CD, circular dichroism; CT, calf thymus; DMSO, dimethyl sulfoxide; ESI, electrospray ionization; ICD, induced circular dichroism; L, linear; *r*, dye to DNA bp molar ratio; TAE, tris-acetate-ethylenediaminetetraacetic acid; *T<sub>m</sub>*, melting temperature; N, nicked; ROS, reactive oxygen species; S, supercoiled.

## REFERENCES

- (1) Zhang, Y., and Galoppini, E. (2010) Organic polyaromatic hydrocarbons as sensitizing model dyes for semiconductor nanoparticles. *ChemSusChem* **3**, 410–428.
- (2) Jarikov, V. V. (2008) Quantum efficiency improvement in anthracene-based organic light-emitting diodes codoped with a hole-trapping material. *Appl. Phys. Lett.* **92**, 244103/1–244103/3.
- (3) Gunnlaugsson, T., Ali, H. D. P., Glynn, M., Kruger, P. E., Hussey, G. M., Pfeffer, F. M., Santos, C. M. G., and Tierney, J. (2005) Fluorescent photoinduced electron transfer (PET) sensors for anions; from design to potential application. *J. Fluoresc.* **15**, 287–299.
- (4) Lodeiro, C., Lippolis, V., and Mameli, M. (2010) From Macrocyclic Ligands to Fluorescent Molecular Sensors for Metal Ions: Recent Results and Perspectives, in *Macrocyclic Chemistry: New Research Developments* (Fitzpatrick, D. W., and Ulrich, H. J., Eds.) pp 159–212, Nova Publishers, Hauppauge, NY.
- (5) Bowden, G. T., Roberts, R., Alberts, D. S., Peng, Y. M., and Garcia, D. (1985) Comparative molecular pharmacology in leukemic L1210 cells of the anthracene anticancer drugs mitoxantrone and bisantrene. *Cancer Res.* **45**, 4915–4920.
- (6) Iyengar, B. S., Dorr, R. T., Alberts, D. S., Sólyom, A. M., Krutzsch, M., and Remers, W. A. (1997) 1,4-disubstituted anthracene antitumor agents. *J. Med. Chem.* **40**, 3734–3738.
- (7) Wilson, W. D., Wang, Y. H., Kusuma, S., Chandrasekaran, S., and Boykin, D. W. (1986) The effect of intercalator structure on binding strength and base-pair specificity in DNA interactions. *Biophys. Chem.* **24**, 101–109.
- (8) Modukuru, N. K., Snow, K. J., Perrin, B. S. Jr., Bhambhani, A., Duff, M., and Kumar, C. V. (2006) Tuning the DNA binding modes of an anthracene derivative with salt. *J. Photochem. Photobiol. A* **177**, 43–54.
- (9) Tan, W. B., Bhambhani, A., Duff, M. R., Rodger, A., and Kumar, C. V. (2006) Spectroscopic identification of binding modes of anthracene probes and DNA sequence recognition. *Photochem. Photobiol.* **82**, 20–30.
- (10) Holmes, F. A., Esparza, L., Yap, H. Y., Buzdar, A. U., Blumenschein, G. R., and Hortobagyi, G. N. (1986) A comparative study of bisantrene given by two dose schedules in patients with metastatic breast cancer. *Cancer Chemother. Pharmacol.* **18**, 157–161.
- (11) Morschhauser, F., Mounier, N., Sebban, C., Brice, P., Solal-Celigny, P., Tilly, H., Feugier, P., Fermé, C., Copin, M. C., and Lamy, T. (2010) Efficacy and safety of the combination of rituximab, fludarabine, and mitoxantrone for rituximab-naïve, recurrent/refractory follicular non-Hodgkin lymphoma with high tumor burden: a multicenter phase 2 trial by the Groupe d'Etude des Lymphomes de l'Adulte (GELA) and Groupe Ouest Est des Leucémies et Autres Maladies du Sang (GOELAMS). *Cancer* **116**, 4299–4308.
- (12) Parker, C., Waters, R., Leighton, C., Hancock, J., Sutton, R., Moorman, A. V., Ancliff, P., Morgan, M., Masurekar, A., Goulden, N., Green, N., Révész, T., Darbyshire, P., Love, S., and Saha, V. (2010)

- Effect of mitoxantrone on outcome of children with first relapse of acute lymphoblastic leukaemia (ALL R3): an open-label randomised trial. *Lancet* 376, 2009–2017.
- (13) de Bono, J. S., Oudard, S., Ozguroglu, M., Hansen, S., Machiels, J. P., Kocak, I., Gravis, G., Bodrogi, I., Mackenzie, M. J., Shen, L., Roessner, M., Gupta, S., and Sartor, A. O. (2010) Prednisone plus cabazitaxel or mitoxantrone for metastatic castration-resistant prostate cancer progressing after docetaxel treatment: a randomised open-label trial. *Lancet* 376, 1147–1154.
- (14) Tuveson, R. W., Wang, G. R., Wang, T. P., and Kagan, J. (1990) Light-dependent cytotoxic reactions of anthracene. *Photochem. Photobiol.* 52, 993–1002.
- (15) Huang, Y., Zhang, Y., Zhang, J., Zhang, D. W., Lu, Q.-S., Liu, J.-L., Chen, S.-Y., Lin, H.-H., and Yu, X.-Q. (2009) Synthesis, DNA binding and photocleavage study of novel anthracene-appended macrocyclic polyamines. *Org. Biomol. Chem.* 7, 2278–2285.
- (16) Bernal, M. E., Varon, J., Acosta, P., and Montagnier, L. (2010) Oxidative stress in critical care medicine. *Int. J. Clin. Pract.* 64, 1480–1488.
- (17) Rai, S., Kasturi, C., Grayzar, J., Platz, M. S., Goodrich, R. P., Yerram, N. R., Wong, V., and Tay-Goodrich, B. H. (1993) Dramatic improvements in viral inactivation with brominated psoralens, naphthalenes and anthracenes. *Photochem. Photobiol.* 58, 59–65.
- (18) Kumar, C. V., Tan, W. B., and Betts, P. W. (1997) Hexamminecobalt(III) chloride assisted, visible light induced, sequence dependent cleavage of DNA. *J. Inorg. Biochem.* 68, 177–181.
- (19) Kumar, C. V., Punzalan, E. H. A., and Tan, W. B. (2000) Adenine-thymine base pair recognition by an anthryl probe from the DNA minor groove. *Tetrahedron* 56, 7027–7040.
- (20) Gude, L., Fernández, M.-J., Grant, K. B., and Lorente, A. (2002) Anthracene and naphthalene (2,2'-bipyridine)platinum(II) conjugates: synthesis and DNA photocleavage. *Tetrahedron Lett.* 43, 4723–4727.
- (21) Gude, L., Fernández, M.-J., Grant, K. B., and Lorente, A. (2005) Syntheses and copper(II)-dependent DNA photocleavage by acridine and anthracene 1,10-phenanthroline conjugate systems. *Org. Biomol. Chem.* 3, 1856–1862.
- (22) Naora, H., Naora, H., Izawa, M., Allfrey, V. G., and Mirsky, A. E. (1962) Some observations on differences in composition between the nucleus and cytoplasm of the frog oocyte. *Proc. Natl. Acad. Sci. U. S. A.* 48, 853–859.
- (23) Billett, M. A., and Barry, J. M. (1974) Role of histones in chromatin condensation. *Eur. J. Biochem.* 49, 477–484.
- (24) Hooper, G., and Dick, D. A. T. (1976) Nonuniform distribution of sodium in the rat hepatocyte. *J. Gen. Physiol.* 67, 469–474.
- (25) Moore, R. D., and Morrill, G. A. (1976) A possible mechanism for concentrating sodium and potassium in the cell nucleus. *Biophys. J.* 16, 527–533.
- (26) Schelhorn, T., Kretz, S., and Zimmermann, H. W. (1992) Reinvestigation of the binding of proflavine to DNA. Is intercalation the dominant binding effect? *Cell. Mol. Biol.* 38, 345–365.
- (27) Bhattacharya, S., and Mandal, S. S. (1997) Interaction of surfactants with DNA. Role of hydrophobicity and surface charge on intercalation and DNA melting. *Biochim. Biophys. Acta* 1323, 29–44.
- (28) Haq, I., Ladbury, J. E., Chowdhry, B. Z., Jenkins, T. C., and Chaires, J. B. (1997) Specific binding of Hoechst 33258 to the d(CGAAATTGCG)<sub>2</sub> duplex: calorimetric and spectroscopic studies. *J. Mol. Biol.* 271, 244–257.
- (29) Manning, G. S. (1972) Application of polyelectrolyte “limiting laws” to the helix-coil transition of DNA. I. Excess univalent cations. *Biopolymers* 11, 937–949.
- (30) Baase, W. A., and Johnson, W. C. (1979) Circular dichroism and DNA secondary structure. *Nucleic Acids Res.* 6, 797–813.
- (31) Belintsev, B. N., Gagua, A. V., and Nedospasov, S. A. (1979) The effect of the superhelicity on the double helix twist angle in DNA. *Nucleic Acids Res.* 6, 983–992.
- (32) Bednar, J., Furrer, P., Stasiak, A., Dubochet, J., Egelman, E. H., and Bates, A. D. (1994) The twist, writhe and overall shape of supercoiled DNA change during counterion-induced transition from a loosely to a tightly interwound superhelix. Possible implications for DNA structure in vivo. *J. Mol. Biol.* 235, 825–847.
- (33) Hamelberg, D., Williams, L. D., and Wilson, W. D. (2001) Influence of the dynamic positions of cations on the structure of the DNA minor groove: sequence-dependent effects. *J. Am. Chem. Soc.* 123, 7745–7755.
- (34) OhUigin, C., McConnell, D. J., Kelly, J. M., and van der Putten, W. J. (1987) Methylene blue photosensitised strand cleavage of DNA: effects of dye binding and oxygen. *Nucleic Acids Res.* 15, 7411–7427.
- (35) Munson, B., and Fiel, R. J. (1992) DNA intercalation and photosensitization by cationic meso substituted porphyrins. *Nucleic Acids Res.* 24, 1080–1090.
- (36) Åckerman, B., and Tuite, E. (1996) Single- and double-strand photocleavage of DNA by YO, YOYO and TOTO. *Nucleic Acids Res.* 20, 1315–1319.
- (37) Grant, K. B., Terry, C. A., Gude, L., Fernández, M.-J., and Lorente, A. (2011) Synthesis and DNA photocleavage by a pyridine-linked bis-acridine chromophore in the presence of copper(II): ionic strength effects. *Bioorg. Med. Chem. Lett.* 21, 1047–1051.
- (38) Newcomb, M., Timko, J. M., Walba, D. M., and Cram, D. J. (1977) Host-guest complexation. 3. Organization of pyridyl binding sites. *J. Am. Chem. Soc.* 99, 6392–6398.
- (39) Sambrook, J., Fritsch, E. F., and Maniatis, T. (1989) *Molecular Cloning: A Laboratory Manual*, 2nd ed., Cold Spring Harbor Laboratory, Cold Spring Harbor, New York.
- (40) Schmid, N., and Behr, J. P. (1991) Location of spermine and other polyamines on DNA as revealed by photoaffinity cleavage with poly(amino)benzenediazonium salts. *Biochemistry* 30, 4357–4361.
- (41) Vedernikov, A. N., Wu, P., Huffman, J. C., and Caulton, K. G. (2002) Cu(I) and Cu(II) complexes of a pyridine-based pincer ligand. *Inorg. Chim. Acta* 330, 103–110.
- (42) Dwyer, T. J., Geierstanger, B. H., Mrksich, M., Dervan, P. B., and Wemmer, D. E. (1993) Structural analysis of covalent peptide dimers, bis(pyridine-2-carboxamidonetrropsin)(CH<sub>2</sub>)<sub>3–6</sub>, in complex with 5'-TGACT-3' sites by two-dimensional NMR. *J. Am. Chem. Soc.* 115, 9900–9906.
- (43) Blackburn, G. M., and Taussig, P. E. (1975) The photocarcinogenicity of anthracene: photochemical binding to deoxyribonucleic acid in tissue culture. *Biochem. J.* 149, 289–291.
- (44) Sinha, B. K., and Chignell, C. F. (1983) Binding of anthracene to cellular macromolecules in the presence of light. *Photochem. Photobiol.* 37, 33–37.
- (45) de Silva, A. P., and de Silva, S. A. (1986) Fluorescent signalling crown ethers; ‘switching on’ of fluorescence by alkali metal ion recognition and binding *in situ*. *J. Chem. Soc., Chem. Commun.*, 1709–1710.
- (46) Kubo, K., Sakurai, T., and Mori, A. (1999) Complexation and fluorescence behavior of 9,10-bis[bis(beta-hydroxyethyl)-aminomethyl]anthracene. *Talanta* 50, 73–77.
- (47) Wilson, B., Gude, L., Fernández, M.-J., Lorente, A., and Grant, K. B. (2005) Tunable DNA photocleavage by an imidazole-acridine conjugate. *Inorg. Chem.* 44, 6159–6173.
- (48) Fernández, M.-J., Wilson, B., Palacios, M., Rodrigo, M. M., Grant, K. B., and Lorente, A. (2007) Copper-activated DNA photocleavage by a pyridine-linked bis-acridine intercalator. *Bioconjugate Chem.* 18, 121–129.
- (49) Oikawa, S., and Kawanishi, S. (1998) Distinct mechanisms of site-specific DNA damage induced by endogenous reductants in the presence of iron(III) and copper(II). *Biochim. Biophys. Acta* 1399, 19–30.
- (50) Sinden, R. R. (1994) *DNA Structure and Function*, pp 109–110, Academic Press, Inc, San Diego.
- (51) Duff, M., Mudhavarthi, V. M., and Kumar, C. V. (2009) Rational design of anthracene-based DNA binders. *J. Phys. Chem. B* 113, 1710–1721.
- (52) Modukuru, N. K., Snow, K. J., Perrin, B. S. Jr., Thota, J., and Kumar, C. V. (2005) Contributions of a long side chain to the binding affinity of an anthracene derivative to DNA. *J. Phys. Chem. B* 109, 11810–11818.

- (53) Cantor, C., and Schimmel, P. R. (1980) *Biophysical Chemistry*, p 398, W.H. Freeman, San Francisco.
- (54) Tuite, E. M., and Kelly, J. M. (1993) Photochemical interactions of methylene blue and analogues with DNA and other biological substrates. *J. Photochem. Photobiol. B* 21, 103–124.
- (55) Dixon, D. W., and Steullet, V. (1998) Dimerization of tetracationic porphyrins: ionic strength dependence. *J. Inorg. Biochem.* 69, 25–32.
- (56) Bolte, J., Demuyncck, C., Lhomme, M. F., Lhomme, J., Barbet, J., and Roques, B. P. (1982) Synthetic models related to DNA intercalating molecules: comparison between quinacrine and chloroquine in their ring-ring interaction with adenine and thymine. *J. Am. Chem. Soc.* 104, 760–765.
- (57) Kumar, C. V., and Asuncion, E. H. (1993) DNA binding studies and site selective fluorescence sensitization of an anthryl probe. *J. Am. Chem. Soc.* 115, 8547–8553.
- (58) Wilson, W. D., Tanious, F. A., and Fernández-Saiz, M. (1997) Evaluation of Drug-Nucleic Acid Interactions by Thermal Melting Curves, in *Drug-DNA Interaction Protocols* (Fox, K. R., Ed.) pp 219–240, Humana Press, Clifton, NJ.
- (59) Gotoh, O., Wada, A., Tada, M., and Tada, M. (1978) Base and base sequence specificity of the binding of 4-hydroxyaminoquinoline 1-oxide to DNA. *Gann* 69, 61–66.
- (60) Duguid, J. G., Bloomfield, V. A., Benevides, J. M., and Thomas, G. J. Jr. (1995) Raman spectroscopy of DNA-metal complexes. II. The thermal denaturation of DNA in the presence of  $\text{Sr}^{2+}$ ,  $\text{Ba}^{2+}$ ,  $\text{Mg}^{2+}$ ,  $\text{Ca}^{2+}$ ,  $\text{Mn}^{2+}$ ,  $\text{Co}^{2+}$ ,  $\text{Ni}^{2+}$ , and  $\text{Cd}^{2+}$ . *Biophys. J.* 69, 2623–2641.
- (61) Novakova, O., Chen, H., Vrana, O., Rodger, A., Sadler, P. J., and Brabec, V. (2003) DNA interactions of monofunctional organometallic ruthenium(II) antitumor complexes in cell-free media. *Biochemistry* 42, 11544–11554.
- (62) Khan, A. U. (1976) Singlet molecular oxygen. A new kind of oxygen. *J. Phys. Chem.* 80, 2219–2228.
- (63) Poulos, A. T., Kuzmin, V., and Geacintov, N. E. (1982) Probing the microenvironment of benzo[a]pyrene diol epoxide-DNA adducts by triplet excited state quenching methods. *J. Biochem. Biophys. Methods* 6, 269–281.